achieved only with 2.55 μM ZOL (Fig. 1E, bars). It is notable that when the viability of the cells in this experiment was assessed with the MTT assay, a 50% reduction in viability was achieved with 7.36 μM ZOL (Fig. 1E, line plot).

3.3. Effect of ZOL on LM8 metastasis-related factors

To examine whether ZOL exerts anti-metastatic effects on OS cells, we investigated its ability to inhibit the migration, adhesion and invasion of LM8 cells during 24 h of culture. In this analysis, non-toxic doses were used as determined by examining LM8 cell viability after 24 h incubation with various concentrations of ZOL in serum-free medium. This revealed that ZOL did not exert a statistically significant effect on LM8 proliferation at concentrations up to 2.5 μM (data not shown). A migration assay performed with LM8 cells and various concentrations of ZOL up to 2 μM revealed that ZOL concentrations of 1 μM or higher significantly blocked LM8 cell migration towards a chemoattractant (Fig. 2A). In addition, ZOL concentrations of 0.5 μM or higher blocked both LM8 cell adhesion on collagen type I-coated plates (Fig. 2B) and LM8 cell invasion of Matrigel towards a chemoattractant (Fig. 2C).

3.4. Effect of ZOL on primary engrafted tumor growth

Before the initiation of mouse experiments, we confirmed that there was no significant difference in the cell characteristics such as proliferation and morphology between the $LM8^{Luc}$ transfected cells and the parent LM8 cell line (data not shown). Mice were injected in the subcutaneous soft tissue of the lateral lumbar region with $LM8^{Luc}$ cells and were either left untreated [group (i)] or were treated with 80 μg/kg ZOL once a week for 4 weeks [group (ii)] or with 80 μg/kg ZOL on the first 3 days of each week for 4 weeks [group (iii)]. We evaluated the efficacy of ZOL over time after inoculation by measuring both the photons of the primary site (Fig. 3A–C) and the tumor volume {data not shown because tumor volumes correlated well with the photons as previously observed [19,24]}. By week 4 of treatment, while the lower dose of ZOL had not affected cell proliferation at the primary site, the higher dose strongly reduced the photons ($p = 0.010$; Fig. 3D). Histological analysis revealed that the primary tumors of group (iii) mice (Fig. 3F) showed many areas of necrosis and calcification, whereas this was not observed in the primary tumors of the control mice (Fig. 3E). Since ZOL inhibited LM8 VEGF production *in vitro* at clinically relevant concentrations (Fig. 1E), we also investigated whether ZOL inhibited the angiogenesis induced by LM8 cells *in vivo* by immunohistochemical analysis of SMA. The group (iii) primary tumors had significantly fewer SMA-positive areas (Fig. 3H and I) than the control tumors (Fig. 3G).

3.5. Effect of ZOL on lung metastasis

Spontaneous lung metastases were observed in all groups by the second week after LM8 cell inoculation (Fig. 4A and C). However, the growth of these metastases after 4 weeks of ZOL treatment was significantly inhibited in group (iii) (Fig. 4B and D). Interestingly, the lower dose of ZOL also reduced the growth of lung metastases (Fig. 4B), even though it barely affected the growth of the primary tumors (Fig. 3D).

4. Discussion

Based on preclinical studies [4,25], several randomized clinical trials have examined the anti-tumor effects of BPs, including the prevention of bone metastases, in breast cancer, and prostate cancer patients [26,27]. However, to our knowledge, clinical trials examining the anti-tumor effects of BPs on OS have not yet been conducted.

ZOL is an inhibitor of farnesyl pyrophosphate (FPP) synthase, and its administration depletes FPP and its downstream metabolite geranylgeranyl diphosphate (GGPP),

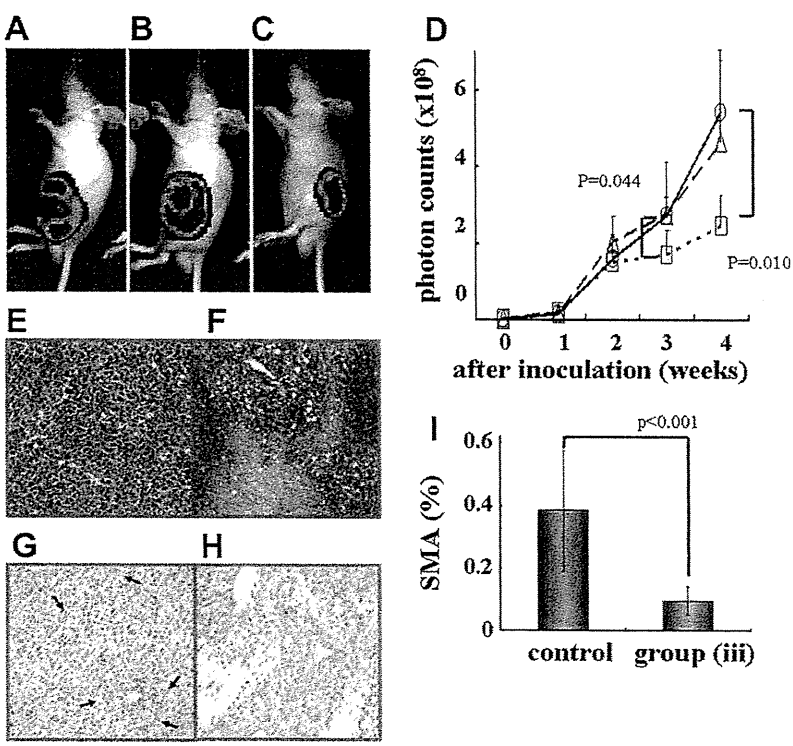

Fig. 3. Effect of ZOL on the *in vivo* growth of OS cells at the primary site. Luc-labeled OS cells ($LM8^{Luc}$) were implanted into the subcutaneous tissue of the lateral lumbar region and monitored by IVIS100. (A–C) IVIS images of mice that were left untreated (A) or were treated with ZOL once a week (B) or for three sequential days every week [C; group (iii)]. The images were taken 4 weeks after inoculation. (D) Mean real-time photon count curves (D) of the primary lesion. Untreated (○); treated with ZOL once a week (△); treated with ZOL on three sequential days a week (□). (E–H) Histological (E and F) and immunohistochemical (G and H) analyses of the primary tumor on week 4 after inoculation from untreated mice (E and G) and mice treated with ZOL for three sequential days a week (F and H). For histological and immunohistochemical analysis, the sections were stained with HE and SMA, respectively. The SMA-positive areas are indicated by the arrows. (I) The SMA-positive areas in G and H were calculated from 10 randomly chosen microscopic fields.

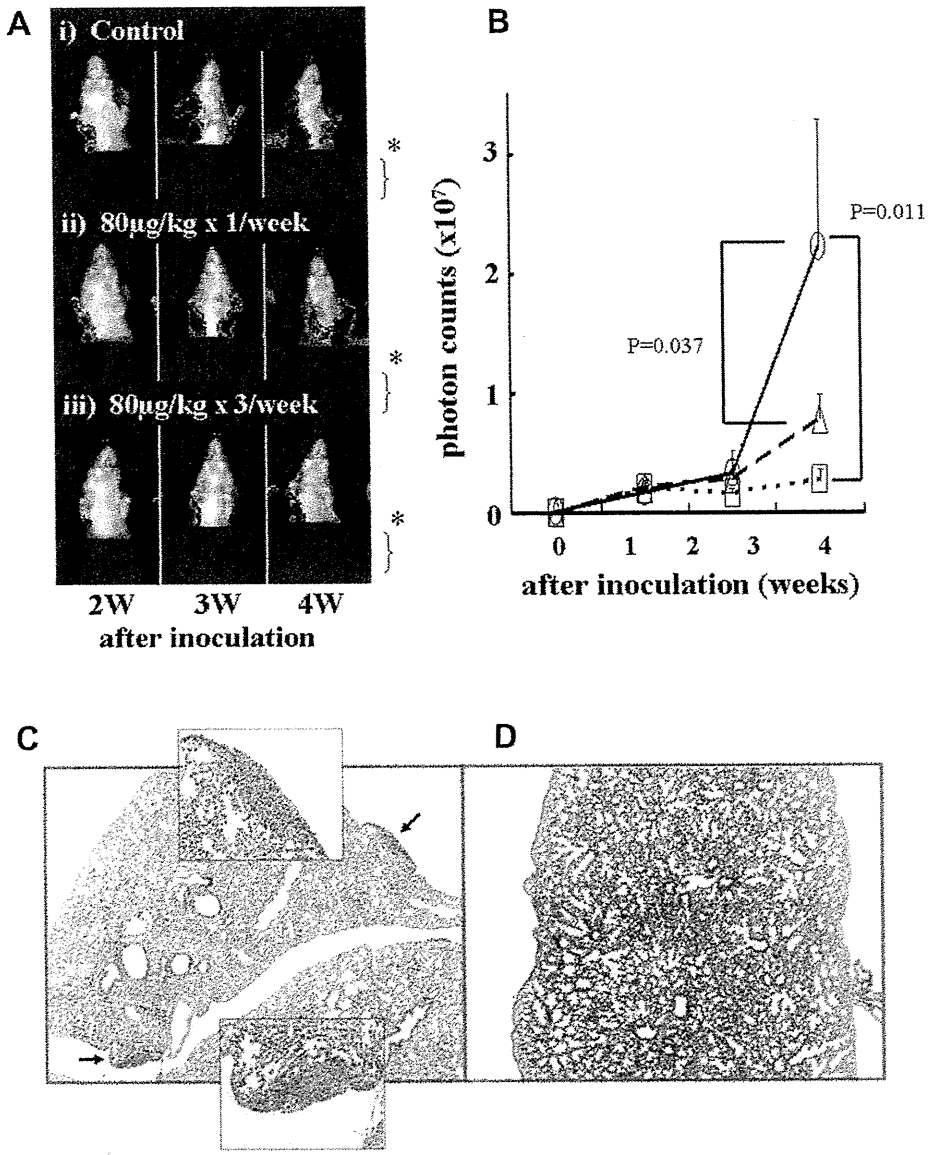

Fig. 4. Effect of ZOL on spontaneous lung metastasis. (A) Lung metastatic lesions in (i) untreated, (ii) treated with ZOL once a week, and (iii) treated with ZOL 3 days a week were monitored by IVIS100. (B) Mean real-time photon curves of metastasis. Untreated (○); treated with ZOL once a week (△); treated with ZOL 3 days a week (□). (C and D) Histological findings of the week 4 HE-stained lungs of untreated mice (C) and mice treated with ZOL for 3 days a week (D). The arrow pointing at the metastasis lesion, and the high power fields are shown in the control group. On the contrary, there is no obvious metastasis lesion in the excised lung of the mice treated with ZOL.

which are essential for the prenylation of small GTPases and thus the activation of Ras family proteins [28]. We showed that treatment of LM8 cells with 10 μM ZOL not only inhibited cell growth (Fig. 1A) and altered the cell cycle (Fig. 1D), but it also induced the accumulation of unprenylated Rap1A (Fig. 1C). Moreover, treatment with GGOH partially reversed the inhibitory effects of 10 μM ZOL on cell proliferation (Fig. 1B). These findings suggest that the anti-proliferative effects of ZOL against LM8 cells are due to interruption of the mevalonate pathway, thereby inhibiting prenylation of Ras family proteins. Similar observations have been made in other cancer cells [4,25].

The anti-proliferative IC_{50} value of ZOL for LM8 cells was less than that reported previously for other cancer cell lines [5–8,25]. BPs are non-hydrolyzable pyrophosphate analogs that strongly bind to hydroxyapatite, which is the main component of bone and teeth [29]. The sensitivity of different cell types to BPs probably depends largely on their ability to internalize sufficient amounts of BPs. Thus, OS, which is defined as an osteoid or bony matrix-producing malignant bone tumor [30], may be more sensitive to BPs than other cancer cells.

ZOL also might have another anti-tumor activity, since we found that it inhibited LM8 VEGF production. Significantly, this activity was exerted by 1–2 μM ZOL, which was lower than the 5–10 μM ZOL concentration needed to inhibit LM8 proliferation (Fig. 1E). VEGF is one of the most potent angiogenic factors known and its expression increases vascular permeability and promotes extravasation of proteins from tumor vessels [31]. Inhibition of VEGF

suppresses tumor growth *in vivo* [32]. BPs have been shown in a previous study to exert anti-angiogenic effects [33]. In the present study, we also found that non-toxic doses of ZOL inhibited not only VEGF production but also the migration, adhesion, and invasion of LM8 cells (Fig. 2). These findings indicate that even if the clinical serum concentration of ZOL does not reach the concentration needed to prevent OS proliferation at the primary site, ZOL may still be useful in preventing metastasis.

It is unclear which molecules consist of Ras family proteins such as Ras, Rho and Rap1, etc. mediate the anti-metastatic effects of ZOL. Since a Ras farnesylation inhibitor reduces cancer metastasis [34], and active Rho is required for variety of complex morphogenetic processes [35], the effects of ZOL on Ras and Rho may, at least in part, mediate its anti-metastatic effects. However, Ras and Rho inhibition only partly explains the anti-metastatic effects of ZOL because 1–2 μM ZOL did not induce a detectable accumulation of unprenylated Ras family protein (Fig. 1C), while this concentration was sufficient to inhibit metastasis-related factors (Fig. 2). Thus, other, non-Ras family protein, targets might be involved. Indeed, van Beek et al. suggested that pamidronate had an additional, as yet unidentified, molecular target in osteoclasts [36]. Furthermore, Monkonnen et al. recently reported that the inhibition of FPP synthase caused the accumulation of the upstream substrate isopentenyl pyrophosphate; this then became conjugated to AMP to form a novel ATP analog that inhibited mitochondrial adenine nucleotide translocase and induced osteoclast apoptosis [37]. Thus, comprehensive identification of the targets of ZOL will be needed to understand how ZOL inhibits metastasis.

Several studies in mouse models have shown that treatment with BPs can inhibit metastasis *in vivo* [9–11]. However, in two of these studies, the mouse models used involved the intravenous inoculation of cancer cells, which meant that the extravasation step from primary tumors was not needed for metastasis. In contrast, Hiraga et al. used a mouse model involving orthotopic inoculation of breast cancer cells. They showed that these cancer cells spontaneously metastasized to bone, liver and lung and that ZOL markedly inhibited this process. However, studies investigating the ability of BPs to prevent the lung metastasis of OS cells have not been performed until now (Fig. 4A).

Although ZOL clearly has the potential to be an anti-tumor drug [5–11], it remains unclear whether the serum concentrations of this agent achieved in humans *in vivo* are sufficient to exert a clinically relevant anti-tumor effect. In humans, ZOL is administered once every 3–4 weeks at an approved dose of 4 mg/patient. This results in peak serum concentrations in the range of 1–2 μM [38]. The clinical ZOL dose of 4 mg per nominal 65 kg body weight is equivalent to approximately 100 μg/kg of the research grade disodium salt of ZOL [11]. Thus, mice given 80 μg/kg ZOL once a week for 4 weeks had a cumulative dose of 320 μg/kg per month, which is 3.2 times the human dose. We found that this dose of ZOL could not inhibit the growth and neovascularization of the primary LM8 tumor (Fig. 3). Only the higher dose of ZOL, namely, 80 μg/kg ZOL given three times a week for 4 weeks (9.6 times the human dose), could inhibit proliferation and neovascularization of subcutaneous OS. This indicates that, in humans, it may be difficult to achieve the high serum concentrations needed for ZOL to inhibit OS proliferation in soft tissue. However, ZOL may still be useful clinically because we found that the lower dose of ZOL could significantly prevent lung metastasis (Fig. 4). Moreover, Daubiné et al. showed (albeit in a mouse model that does not recapitulate all the steps required for spontaneous metastasis) that a cumulative dose of ZOL of 100 μg/kg per month significantly inhibited bone metastasis in a mouse model [10]. It is conceivable that the lower dose we used approximates to the dose used in humans since bone turnover in rodents is three to five times higher than that in humans. Thus, it could be argued that fivefold higher BP doses in animal models of bone metastasis will mimic the clinical situation in humans [39]. This conclusion is supported by the observation that BPs given at the standard 4 mg reduce circulating VEGF levels in cancer patients [40]. Thus, the standard dose of ZOL in humans may be theoretically able to inhibit OS lung metastasis.

In current clinical OS surgery, we are frequently obliged by necessity to salvage the limbs of OS patients and need neoadjuvant chemotherapy to prevent the risk of later metastasis despite incomplete effects. Since ZOL is safe and well tolerated and rarely causes irreversible adverse events, even upon long-term use, our results suggest that ZOL may be useful for preventing lung metastasis in OS patients when accompanied with surgical resection of the primary site. Moreover, the use of ZOL in combination with adjuvant therapy and anti-cancer agents may also improve the outcome of OS patients. Supporting this are the reports by us and others that ZOL can act synergistically with a variety of currently used anti-cancer agents, at least *in vitro* [13,41,42]. For example, Mitsiades et al. have recently reported that with androgen ablation-refractory metastatic prostate cancer patients under androgen ablation, ZOL combined with dexamethasone and a somatostatin analog achieves palliative clinical responses superior to those generated by ZOL alone [43].

In conclusion, the lower concentration of ZOL which is achievable in the clinic showed anti-metastatic effects *in vitro* on OS cells. *In vivo*, the high dose of ZOL inhibited both OS growth at the primary site and metastases from the primary site. Interestingly, a lower dose of ZOL which may be achievable in humans significantly prevented lung metastasis despite no effects at the primary site. These finding may provide a rationale to use ZOL for the prevention of lung metastasis when accompanied with surgical resection of primary OS.

Conflict of interest

All authors have nothing to declare about the conflict of interest.

Acknowledgements

We are grateful to Dr. Jonathan Green (Novartis Pharma AG, Basel, Switzerland) for critically reading the manu-

script and to Ms. Yoko Nakagawa for her excellent technical support. This study is partially supported by Grants-in-Aid for Scientific Research from the Ministry of Education, Culture, Sports, Science and Technology of Japan (15790796 to H.M. and 18591056 to S.K.).

References

[1] C.A. Arndt, W.M. Crist, Common musculoskeletal tumors of childhood and adolescence, N. Engl. J. Med. 341 (1999) 342–352.
[2] G. Bacci, S. Ferrari, A. Longhi, et al, Pattern of relapse in patients with osteosarcoma of the extremities treated with neoadjuvant chemotherapy, Eur. J. Cancer 37 (2001) 32–38.
[3] B. Kempf-Bielack, S.S. Bielack, H. Jürgens, et al, Osteosarcoma relapse after combined modality therapy: an analysis of unselected patients in the Cooperative Osteosarcoma Study Group (COSS), J. Clin. Oncol. 23 (2005) 559–568.
[4] J.R. Green, Bisphosphonates: preclinical review, Oncologist 9 (2004) 3–13.
[5] J. Kuroda, S. Kimura, H. Segawa, et al, The third-generation bisphosphonate zoledronate synergistically augments the anti-Ph+ leukemia activity of imatinib mesylate, Blood 102 (2003) 2229–2235.
[6] S. Matsumoto, S. Kimura, H. Segawa, et al, Efficacy of the third-generation bisphosphonate, zoledronic acid alone and combined with anti-cancer agents against small cell lung cancer cell lines, Lung Cancer 47 (2005) 31–39.
[7] T. Yuasa, M. Nogawa, S. Kimura, et al, A third-generation bisphosphonate, minodronic acid (YM529), augments the interferon alpha/beta-mediated inhibition of renal cell cancer cell growth both in vitro and in vivo, Clin. Cancer Res. 11 (2005) 853–859.
[8] K. Sato, T. Yuasa, M. Nogawa, et al, A third-generation bisphosphonate, minodronic acid (YM529), successfully prevented the growth of bladder cancer in vitro and in vivo, Br. J. Cancer 95 (2006) 1354–1361.
[9] T. Hiraga, P.J. Williams, A. Ueda, D. Tamura, T. Yoneda, Zoledronic acid inhibits visceral metastases in the 4T1/luc mouse breast cancer model, Clin. Cancer Res. 10 (2004) 4559–4567.
[10] F. Daubiń, C. Le Gall, J. Gasser, J. Green, P. Clèzrdin, Antitumor effects of clinical dosing regimens of bisphosphonates in experimental breast cancer bone metastasis, J. Natl. Cancer Inst. 99 (2007) 322–330.
[11] B. Ory, M.F. Heymann, A. Kamijo, F. Gouin, D. Heymann, F. Redini, Zoledronic acid suppresses lung metastases and prolongs overall survival of osteosarcoma-bearing mice, Cancer 104 (2005) 2522–2529.
[12] N. Horie, H. Murata, Y. Nishigaki, et al, The third-generation bisphosphonates inhibit proliferation of murine osteosarcoma cells with induction of apoptosis, Cancer Lett. 238 (2006) 111–118.
[13] N. Horie, H. Murata, S. Kimura, et al, Combined effects of a third-generation bisphosphonate, zoledronic acid with other anti-cancer agents against osteosarcoma, Brit. J. Cancer 96 (2007) 255–261.
[14] K. Unni, Dahlin's Bone Tumors: General Aspects & Data on 11087 Cases, fifth ed., Lippincott-Raven, Philadelphia, PA, 1996.
[15] T. Asai, T. Ueda, K. Itoh, et al, Establishment and characterization of a murine osteosarcoma cell line (LM8) with high metastatic potential to the lung, Int. J. Cancer 76 (1998) 418–422.
[16] J. Yang, S.A. Mani, J.L. Donaher, et al, Twist, a master regulator of morphogenesis, plays an essential role in tumor metastasis, Cell 117 (2004) 927–939.
[17] I.J. Fidler, The pathogenesis of cancer metastasis: the seed and soil hypothesis revisited, Nat. Rev. Cancer 3 (2003) 453–458.
[18] M. Nogawa, T. Yuasa, S. Kimura, et al, Zoledronic acid mediates Ras-independent growth inhibition of prostate cancer cells, Oncol. Res. 15 (2005) 1–9.
[19] M. Nogawa, T. Yuasa, S. Kimura, et al, Monitoring luciferase-labeled cancer cell growth and metastasis in different in vivo models, Cancer Lett. 217 (2005) 243–253.
[20] H. Takeshita, K. Kusuzaki, Y. Tsuji, et al, Avoidance of doxorubicin resistance in osteosarcoma cells using a new quinoline derivative, MS-209, Anticancer Res. 18 (1998) 739–742.
[21] S. Kimura, T. Maekawa, K. Hirakawa, A. Murakami, T. Abe, Alterations of c-myc expression by antisense oligodeoxynucleotides enhance the induction of apoptosis in HL-60 cells, Cancer Res. 55 (1995) 1379–1384.
[22] M. Nogawa, T. Yuasa, S. Kimura, et al, Intravesical administration of small interfering RNA targeting PLK-1 successfully prevents the growth of bladder cancer, J. Clin. Invest. 115 (2005) 978–985.
[23] T. Ueda, N. Araki, M. Mano, et al, Frequent expression of smooth muscle markers in malignant fibrous histiocytoma of bone, J. Clin. Pathol. 55 (2002) 853–858.
[24] K. Sato, S. Kimura, H. Segawa, et al, Cytotoxic effects of γδ T cells expanded ex vivo by a third generation bisphosphonate for cancer immunotherapy, Int. J. Cancer 116 (2005) 94–99.
[25] A.J. Roelofs, K. Thompson, S. Gordon, M.J. Rogers, Molecular mechanisms of action of bisphosphonates: current status, Clin. Cancer Res. 12 (2006) 6222–6230.
[26] R.E. Coleman, Bisphosphonates for the prevention of bone metastases, Semin. Oncol. 29 (2002) 43–49.
[27] K. Mystakidou, E. Katsouda, E. Parpa, A. Kelekis, A. Galanos, L. Vlahos, Randomized, open label, prospective study on the effect of zoledronic acid on the prevention of bone metastases in patients with recurrent solid tumors that did not present with bone metastases at baseline, Med. Oncol. 22 (2005) 195–201.
[28] J.E. Dunford, K. Thompson, F.P. Coxon, et al, Structure–activity relationships for inhibition of farnesyl diphosphate synthase in vitro and inhibition of bone resorption in vivo by nitrogen-containing bisphosphonates, J. Pharmacol. Exp. Ther. 296 (2001) 235–242.
[29] J.R. Green, Skeletal complications of prostate cancer: pathophysiology and therapeutic potential of bisphosphonates, Acta Oncol. 44 (2005) 282–292.
[30] K.K. Unni, Osteosarcoma of bone, J. Orthop. Sci. 3 (1998) 287–294.
[31] H.F. Dvorak, J.A. Nagy, B. Berse, et al, Vascular permeability factor, fibrin, and the pathogenesis of tumor stroma formation, Ann. N.Y. Acad. Sci. 667 (1992) 101–111.
[32] K.J. Kim, B. Li, J. Winer, et al, Inhibition of vascular endothelial growth factor-induced angiogenesis suppresses tumour growth in vivo, Nature 362 (1993) 841–844.
[33] P.S. Fournier, S. Boissier, J. Filleur, et al, Bisphosphonates inhibit angiogenesis in vitro and testosterone-stimulated vascular regrowth in the ventral prostate in castrated rats, Cancer Res. 62 (2002) 6538–6544.
[34] J.S. Nam, Y. Ino, M. Sakamoto, S. Hirohashi, Ras farnesylation inhibitor FTI-277 restores the E-cadherin/catenin cell adhesion system in human cancer cells and reduces cancer metastasis, Jpn. J. Cancer Res. 93 (2002) 1020–1028.
[35] U. Hacker, N. Perrimon, RhoGEF2 encodes a member of the Dbl family of oncogenes and controls cell shape changes during gastrulation in *Drosophila*, Genes Dev. 12 (1998) 274–284.
[36] E.R. van Beek, L.H. Cohen, I.M. Leroy, F.H. Ebetino, C.W. Lowik, S.E. Papapoulos, Differentiating the mechanisms of antiresorptive action of nitrogen containing bisphosphonates, Bone 33 (2003) 805–811.
[37] H. Monkkonen, S. Auriola, P. Lehenkari, et al, A new endogenous ATP analog (AppppI) inhibits the mitochondrial adenine nucleotide translocase (ANT) and is responsible for the apoptosis induced by nitrogen-containing bisphosphonates, Brit. J. Pharmacol. 147 (2006) 437–445.
[38] T. Chen, J. Berenson, R. Vescio, et al, Pharmacokinetics and pharmacodynamics of zoledronic acid in cancer patients with bone metastases, J. Clin. Pharmacol. 42 (2002) 1228–1236.
[39] F. Bauss, M. Wagner, L.H. Hothorn, Total administered dose of ibandronate determines its effects on bone mass and architecture in ovariectomized aged rats, J. Rheumatol. 29 (2002) 990–998.
[40] D. Santini, B. Vincenzi, G. Dicuonzo, et al, Zoledronic acid induces significant and long-lasting modifications of circulating angiogenic factors in cancer patients, Clin. Cancer Res. 9 (2003) 2893–2897.
[41] J.K. Woodward, R.E. Coleman, I. Holen, Preclinical evidence for the effect of bisphosphonates and cytotoxic drugs on tumor cell invasion, Anticancer Drugs 16 (2005) 11–19.
[42] D.R. Budman, A. Calabro, Zoledronic acid (Zometa) enhances the cytotoxic effect of gemcitabine and fluvastatin: in vitro isobologram studies with conventional and nonconventional cytotoxic agents, Oncology 70 (2006) 147–153.
[43] C.S. Mitsiades, J. Bogdanos, D. Karamanolakis, C. Milathianakis, T. Dimopoulos, M. Koutsilieris, Randomized controlled clinical trial of a combination of somatostatin analog and dexamethasone plus zoledronate vs. zoledronate in patients with androgen ablation-refractory prostate cancer, Anticancer Res. 26 (2006) 3693–3700.

β-Catenin Small Interfering RNA Successfully Suppressed Progression of Multiple Myeloma in a Mouse Model

Eishi Ashihara,[1] Eri Kawata,[1] Yoko Nakagawa,[1] Chihiro Shimazaski,[2] Junya Kuroda,[2] Kyoko Taniguchi,[2] Hitoji Uchiyama,[2] Ruriko Tanaka,[1] Asumi Yokota,[1] Miki Takeuchi,[1] Yuri Kamitsuji,[1] Tohru Inaba,[3] Masafumi Taniwaki,[2] Shinya Kimura,[1] and Taira Maekawa[1]

Abstract

Purpose: β-catenin is the downstream effector of the Wnt signaling pathway, and it regulates cell proliferation. β-catenin overexpression correlates positively with prognosis in several types of malignancies. We herein assessed its effects on growth of multiple myeloma cells using a xenograft model.

Experimental Design: We first investigated the expression of β-catenin in multiple myeloma cell lines and multiple myeloma cells obtained from patients. Next, we investigated the growth inhibitory effects of β-catenin small interfering RNA on the growth of multiple myeloma cells *in vivo*. Six-week-old male BALB/c *nu/nu* mice were inoculated s.c. in the right flank with 5×10^6 RPMI8226 cells, followed by s.c. injections of β-catenin small interfering RNA, scramble small interfering RNA, or PBS/atelocollagen complex twice a week for a total of eight injections.

Results: Significantly higher levels of β-catenin expression were observed in multiple myeloma cell lines and in samples from patients with multiple myeloma than those found in mononuclear cells obtained from healthy volunteers. In *in vivo* experiments, no inhibitory effects were observed following treatment with scramble small interfering RNA or PBS/atelocollagen complexes, whereas treatment with β-catenin small interfering RNA/atelocollagen complex significantly inhibited growth of multiple myeloma tumors ($P < 0.05$).

Conclusions: β-catenin small interfering RNA treatment inhibited the growth of multiple myeloma tumors in a xenograft model. To our knowledge, this is the first report showing that the treatment with β-catenin small interfering RNA produces an inhibitory effects on growth of hematologic malignancies *in vivo*. Because treatment with β-catenin small interfering RNA inhibited growth of multiple myeloma cells, β-catenin is the attractive novel target for treating multiple myeloma.

As we gain a better understanding of the pathogenesis underlying multiple myeloma, new molecular targeting agents can be developed. At present, multiple myeloma remains incurable, so it is important to continue to investigate new therapeutic agents that focus on the biology of multiple myeloma cells. β-catenin is the downstream effector of the Wnt signaling pathway, and it regulates the genes encoding cyclin D1 and c-myc (1–3). Activation of Wnt signaling is closely involved in the process of carcinogenesis (4), and β-catenin overexpression has been observed in several types of malignant tumors, including hematologic malignancies (5–9).

RNA interference is a powerful tool in postgenomic research, and recently, experimentally introduced small interfering RNAs have been used in cancer therapy. The success of small interfering RNA therapy depends upon the development of suitable delivery systems, and several useful drug delivery systems have been developed (10–13). Among the drug delivery systems, atelocollagen represents one of the most attractive nonviral carriers for gene delivery. It is obtained from calf dermis, following the removal of immunogenic telopeptides located at the N- and C-termini of collagen molecules. Because atelocollagen has a positively charged surface, it easily binds negatively charged molecules such as nucleic acids. The small interfering RNA/atelocollagen complex is also resistant to nucleases and is transduced efficiently, resulting in long-term gene silencing (14). Here,

Authors' Affiliations: [1]Department of Transfusion Medicine and Cell Therapy, Kyoto University Hospital; [2]Division of Hematology and Oncology, Department of Medicine; and [3]Department of Molecular Genetics and Laboratory Medicine, Kyoto Prefectural University of Medicine, Kyoto, Japan

Received 5/23/08; revised 12/21/08; accepted 1/12/09; published OnlineFirst 4/7/09.

Grant support: Aki Horinouchi Research Grant from the International Myeloma Foundation Japan and by a Grant-in-Aids for Scientific Research from the Ministry of Education, Culture, Sports, Science and Technology of Japan.

The costs of publication of this article were defrayed in part by the payment of page charges. This article must therefore be hereby marked *advertisement* in accordance with 18 U.S.C. Section 1734 solely to indicate this fact.

Note: Supplementary data for this article are available at Clinical Cancer Research Online (http://clincancerres.aacrjournals.org/).

E. Ashihara and E. Kawata contributed equally to this study.

Requests for reprints: Eishi Ashihara, Department of Transfusion Medicine and Cell Therapy, Kyoto University Hospital, 54 Kawahara-cho, Shogoin, Sakyo-ku, Kyoto 606-8507, Japan. Phone: 81-75-751-3630; Fax: 81-75-751-4283; E-mail: ash0325@kuhp.kyoto-u.ac.jp.

doi:10.1158/1078-0432.CCR-08-1350

Translational Relevance

In this study, we showed that β-catenin small interfering RNA treatment successfully inhibited the growth of myeloma cells *in vivo* and we revealed that β-catenin is an attractive target for multiple myeloma. These findings not only show evidences for efficacy of targeting therapies for Wnt/β-catenin pathway but also encourage the possibilities of small interfering RNA therapies against multiple myeloma.

we use a xenograft model to show the inhibitory effect of the β-catenin small interfering RNA/atelocollagen complex on growth of multiple myeloma cells.

Materials and Methods

Cell lines and human samples. The human AMO-1, RPMI8226, NCI-H929, U226, OPM-2, KMS-12-BM, EJM, LP-1 myeloma cell lines, and IM-9 Epstein-Barr virus–transformed cell line derived from multiple myeloma patient were purchased from the Deutsche Sammlung von Mikroorganismen und Zellkulturen GmbH. The IM-9, OPM-2, RPMI8226, NCI-H929, and U266 were cultured in RPMI1640 (Gibco) containing 10% heat-inactivated FCS (Invitrogen), 2 mmol/L L-glutamine (Gibco), and 1% penicillin-streptomycin (Gibco). The AMO-1 and KMS-12-BM cell lines were cultured in RPMI1640 containing 20% FCS, 2 mmol/L L-glutamine, and 1% penicillin-streptomycin. The EJM and LP-1 cell lines were cultured in Iscove's modified Dulbecco's medium (Gibco) containing 10% FCS, 2 mmol/L L-glutamine, and 1% penicillin-streptomycin. All cell lines were maintained at 37°C in a fully humidified atmosphere of 5% CO_2 in air.

Six bone marrow samples, one ascites sample, and two pleural effusion samples were obtained from five multiple myeloma patients. Three bone marrow samples were obtained from healthy volunteers. In accordance with the Declaration of Helsinki recommendations, all procedures were approved by the institutional review board at Kyoto Prefectural University of Medicine, and written informed consent was obtained from every participant.

Expression of β-catenin in multiple myeloma cells. We used Western blotting analysis to investigate the expression of β-catenin in nine human multiple myeloma cell lines, as well as primary multiple myeloma cells. Ficoll-Hypaque density centrifugation was used to separate mononuclear cells from each participant's samples. A magnetic cell sorting separation system (Miltenyi) and anti-CD138 antibody (Miltenyi) were used to enrich multiple myeloma cells and normal plasma cells from bone marrow samples. Cells were analyzed by FACS Calibur using the Cell Quest software (BD Bioscience). The purity of enriched CD138+ cell populations was ≥90%. Multiple myeloma cells from ascites and pleural effusion were shown to express CD138. Cells were lysed with radioimmunoprecipitation assay buffer (50 mmol/L Tris-HCl, pH 7.4; 0.25 mol/L NaCl; 5 mmol/L EDTA; 20 mmol/L NaF; 1% NP-40) containing freshly prepared phenylmethylsulfonylfluoride (1 mmol/L) and protease inhibitor (10 μg/mL). Cell suspensions were cleared by centrifugation at 14,000 × *g* for 30 mins at 4°C. Nuclear and cytoplasmic protein fractions were obtained using by NE-PER Nuclear and Cytoplasmic Extraction Reagents kit (Pierce Biotechnology) according to the manufacturer's instruction. The supernatant (total cell lysate, nuclear, and cytoplasmic protein fractions) was either used immediately or stored at -80°C. Protein concentrations were determined using the DC Protein Assay (Bio-Rad Laboratories). Immunoblotting was done as described previously (15). Samples of cell extracts containing 20 μg of protein were analyzed. As the primary antibodies, we used a mouse monoclonal anti–β-catenin antibody (BD Pharmingen), a mouse anti–dephosphorylated β-catenin monoclonal antibody (Alexis Biochemicals), a mouse anti–phosphorylated β-catenin monoclonal antibody (Sigma-Aldrich), a rabbit polyclonal anti–cleaved caspase-3 antibody (Cell Signaling Technology), a rabbit polyclonal anti–caspase-3 antibody (Cell Signaling Technology), a rabbit polyclonal anti–Oct-1 (Santa Cruz Biotechnology), and a rabbit polyclonal anti-actin antibody (Sigma-Aldrich). Horseradish peroxidase–coupled anti–mouse and anti–rabbit immunoglobulin G (Amersham Biosciences) were used as

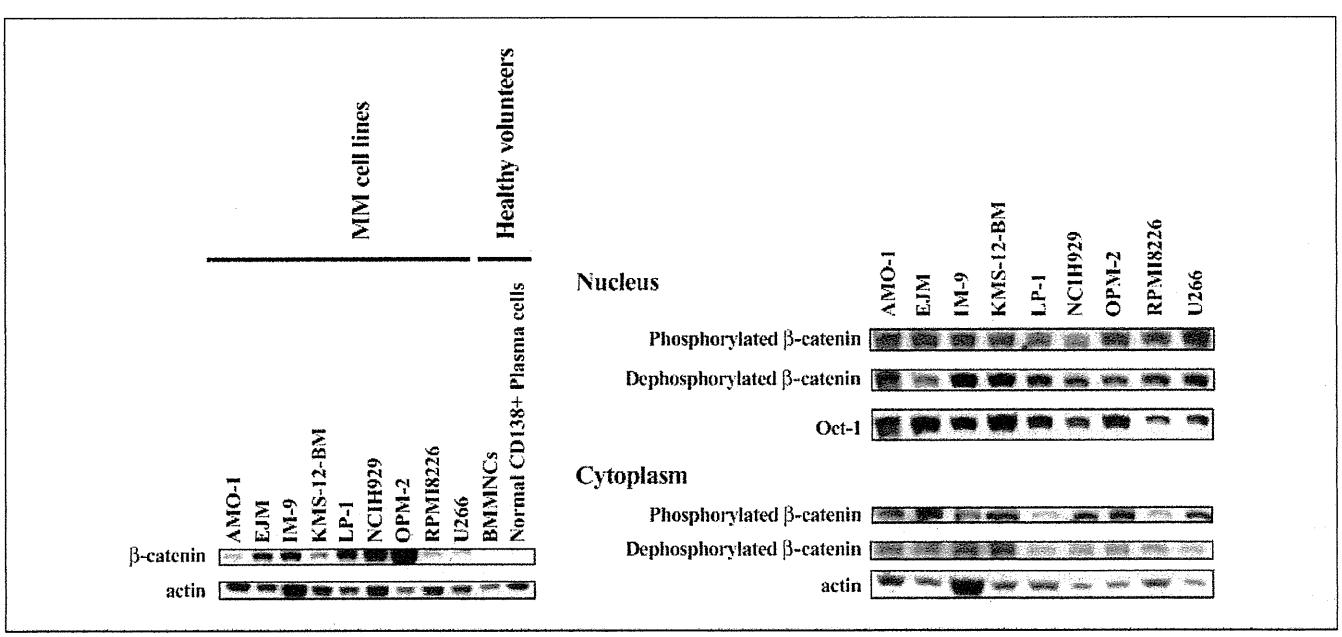

Fig. 1. β-catenin expression in human myeloma cell lines. β-catenin expression was examined by Western blotting. Left, β-catenin was overexpressed in myeloma cell lines and in multiple myeloma patient samples compared with bone marrow mononuclear cells and normal CD138+ plasma cells obtained from healthy volunteers. Actin expression was used as a loading control. Right, phosphorylated and dephosphorylated forms of β-catenin were expressed in multiple myeloma cell lines.

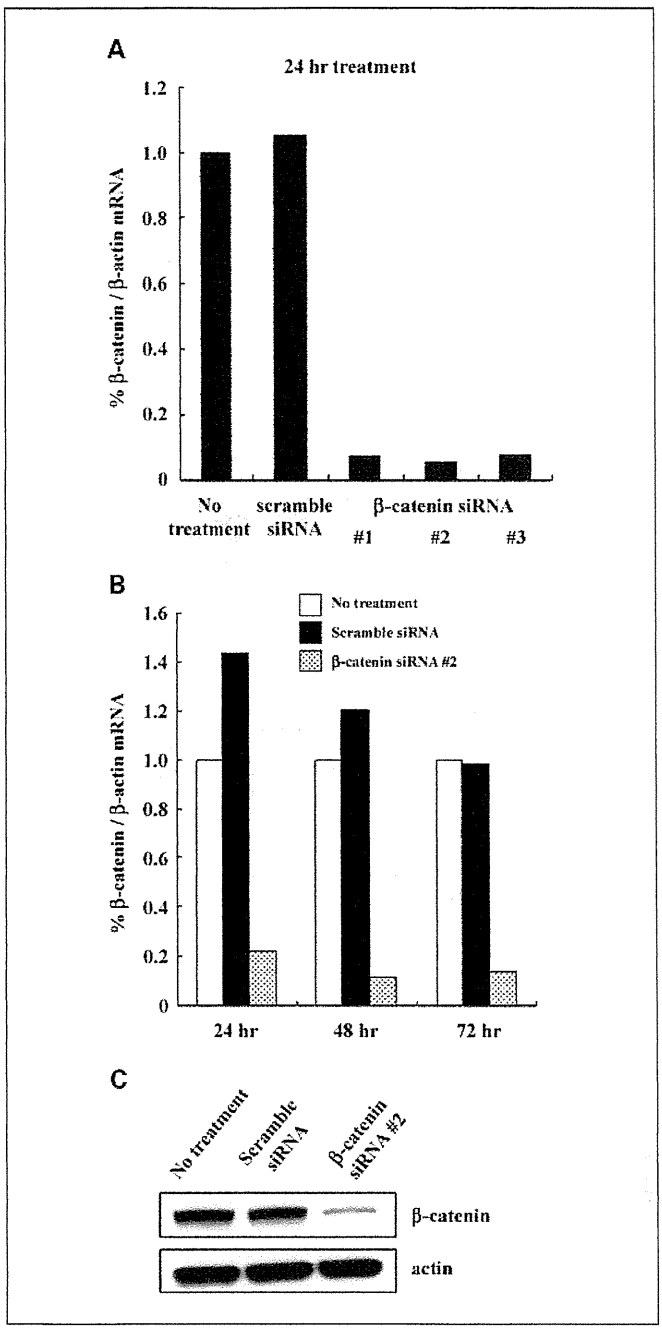

Fig. 2. Effects of β-catenin small interfering RNA *in vitro*. *A*, RT-PCR analysis. All three β-catenin small interfering RNAs decreased *β-catenin* mRNA levels in SW480 cells after 24-h treatment. No reduction in expression was observed for cells with no treatment or treatment with scramble small interfering RNA. *B*, real-time PCR analysis. Treatment of A549 cells with β-catenin small interfering RNA 2 leads to a decrease in *β-catenin* mRNA levels over a period of 72 h. No reduction in expression was observed for cells with no treatment or treatment with scramble small interfering RNA. *C*, Western blotting analysis of A549 cell lysates. There was a decreased expression of β-catenin small interfering RNA after 72-h treatment with β-catenin 2. No reduction in expression was observed for cells with no treatment or treatment with scramble small interfering RNA. Actin expression was used as a loading control.

secondary antibodies, and signal detection was done with an enhanced chemiluminescence kit (Amersham Biosciences).

Effects of knockdown with β-catenin small interfering RNA. Three types of β-catenin (Gene Bank accession number NM_001904) small interfering RNA and one scramble small interfering RNA with the following sense and antisense sequences were used: β-catenin small interfering RNA 1, 5′-CCAGGAUGAUCCUAGCUAUTT-3′ (sense), 5′-AUAGCUAGGAUCAUCCUGGTT-3′ (antisense); β-catenin small interfering RNA 2, 5′- GUAUUUGAAGUAUACCAUATT-3′ (sense), 5′-UAUGGUAUACUUCAAAUACTT-3′ (antisense); β-catenin small interfering RNA 3, 5′- CCAUUACAACUCUCCACAATT-3′ (sense), 5′-UUGUGGAGAGUUGUAAUGGTT-3′ (antisense); and scramble small interfering RNA 2, 5′- GGAAGAUAAUCUUUUCUAATT-3′ (sense), 5′-UUAGAAAAGAUUAUCUUCCTT-3′ (antisense). All small interfering RNAs were synthesized by Takara Bio, Inc. We first examined the effects of small interfering RNA-mediated knockdown using real-time reverse transcription-PCR (RT-PCR) and Western blotting analysis. Following transfection of β-catenin small interfering RNA into SW480 colon cancer cells and A549 lung cancer cells with Lipofectamine 2000 (Invitrogen), total RNA was extracted using the Micro-to-Midi Total RNA Extraction Kit (Invitrogen) and then subjected to reverse transcription (16). The levels of human *β-catenin* mRNA were analyzed using the LightCycler System (Roche Diagnostics) and FastStart DNA Master SYBER Green I (Roche). Amplicons were validated by melting curve and gel electrophoresis. The expression levels of the target mRNAs were normalized to those of the housekeeping gene *β-actin*. The specific primers used for amplification were as follows: *β-catenin*, 5′-GCTTGGTTCACCAGTGGATT (forward) and 3′- CCTTCCAGAGGAACCCTGAG (reverse); and *β-actin*, 5′-GGACTTCGAGCAAGAGATGG (forward) and 3′-GACATGCGGTTGTGTCACGA (reverse). Transfected cells were also examined using Western blotting analysis as described above.

In vivo ***effects of β-catenin small interfering RNA on myeloma tumors.*** After 3 Gy irradiation, specific pathogen-free 6- to 7-wk old male BALB/c *nu/nu* mice (SLC) were inoculated s.c. in the right flank with 5×10^6 RPMI8226 myeloma cells in 100 μL PBS. Palpable tumors (100 mm^3 in volumes) developed within 3 or 4 wks. Mice were then treated with s.c. (around tumors) injections of β-catenin small interfering RNA (2.5 μmol/L)/1% atelocollagen complex (final atelocollagen concentration, 0.5%), scramble small interfering RNA (2.5 μmol/L)/1% atelocollagen complex, β-catenin small interfering RNA (2.5 μmol/L)/PBS, or PBS/1% atelocollagen, twice a week for a total of eight injections. Tumor size was measured in two dimensions using a caliper, and tumor volume (mm^3) was calculated as $a^2 \times b/2$ mm^3 (a, minor axis; b, major axis).

Real-time RT-PCR and immunohistochemical examinations were used to examine the effects of β-catenin small interfering RNA-mediated knockdown in s.c. multiple myeloma tumors. Real-time RT-PCR was done as described above. For immunohistochemical examinations, paraffin-embedded tumor sections were immunolabeled with primary antibodies; that is, mouse β-catenin or anti-c-myc monoclonal antibodies (Santa Cruz Biotechnology), or rabbit polyclonal anti-cleaved caspase-3 antibody (Cell Signaling Technology). Primary antibodies were visualized using the conventional avidin-biotin-peroxidase complex method (VECTASTATIN Elite ABC kit, Vector Laboratories, Inc.). Sections were counterstained with hematoxylin and mounted. Detection of apoptosis was done using the terminal uridine deoxynucleotide nick end labeling (TUNEL) method and an ApopTag plus peroxidase *in situ* apoptosis detection kit (Millipore), according to the manufacturer's instructions. Approval for these studies was obtained from the Committee on Animal Research of the Kyoto University Faculty of Medicine.

Statistical analysis. The *in vivo* effects of small interfering RNA treatment were analyzed using the Student's t test. Values of $P < 0.05$ were considered to be statistically significant.

Results

Expression of β-catenin in myeloma cells. Firstly, we examined human multiple myeloma cell lines, all of which expressed

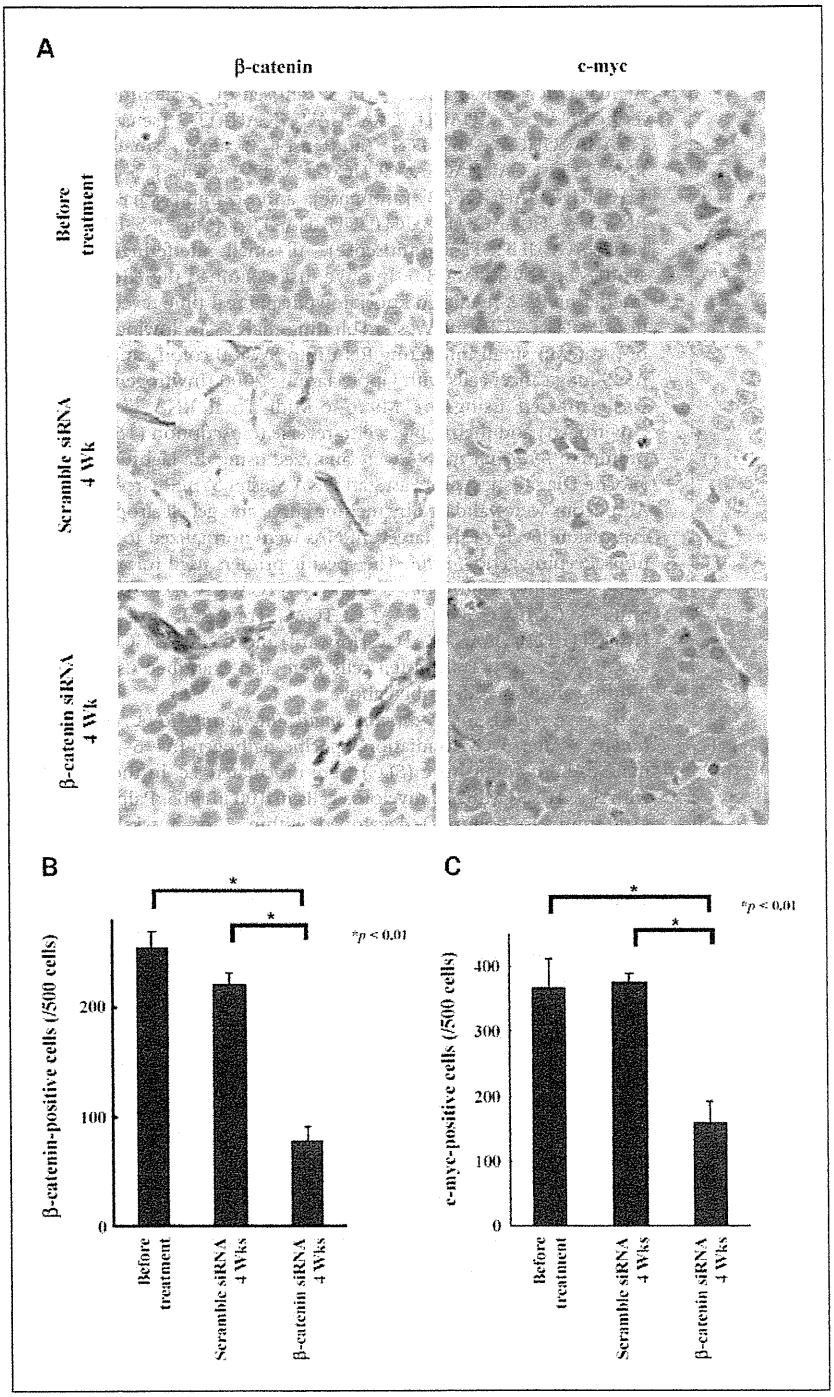

Fig. 3. Changes to β-catenin expression in myeloma tumors following treatment with β-catenin small interfering RNA. *A,* mice ($n = 3$ per group) were treated with s.c. injections of β-catenin small interfering RNA (2.5 μmol/L)/1% atelocollagen complex (final atelocollagen concentration, 0.5%) or scramble small interfering RNA (2.5 μmol/L)/1% atelocollagen complex. Immunohistochemical studies revealed that β-catenin and c-myc expression diminished following 4 wks of treatments with β-catenin small interfering RNA/atelocollagen complex relative to before treatment and with the scramble small interfering RNA/atelocollagen complex. *B,* β-catenin small interfering RNA/atelocollagen complex treatment significantly decreased β-catenin expression in multiple myeloma tumors relative to no treatment and treatment with the scramble small interfering RNA/atelocollagen complex. Results are means ± SEs. *C,* β-catenin small interfering RNA/atelocollagen complex treatment significantly decreased c-myc expression in multiple myeloma tumors relative to no treatment and treatment with the scramble small interfering RNA/telocollagen complex. Results are means ± SEs.

significantly higher β-catenin levels than normal human mononuclear cells and normal plasma cells (Fig. 1, *left*). We investigated phosphorylated and dephosphorylated forms of β-catenin. Both forms of β-catenin were expressed in multiple myeloma cell lines and primary multiple myeloma cells (Fig. 1, *right*). Total β-catenin levels in the cell lines did not correlate with phosphorylated and dephosphorylated β-catenin levels in the nuclear and cytoplasmic fractions. We speculate that the localizations of both β-catenin forms are different and that the degradation rates caused by proteasome are different in various cell lines. Moreover, we found significantly elevated expression of both forms of β-catenin in myeloma cells obtained from patients, relative to cells obtained from healthy volunteers (Supplementary Fig. S1).

Effects of knockdown with β-catenin small interfering RNA. We then examined knockdown of endogenous level of β-catenin protein levels using the three types of β-catenin small interfering RNA. Following transfection β-catenin or scramble small interfering RNA (100 nmol/L) into SW480 cells and A549 cells, we examined β-catenin expression using real-time RT-PCR and Western blot analysis. SW480 cells were examined 24 hours after treatment with the three β-catenin

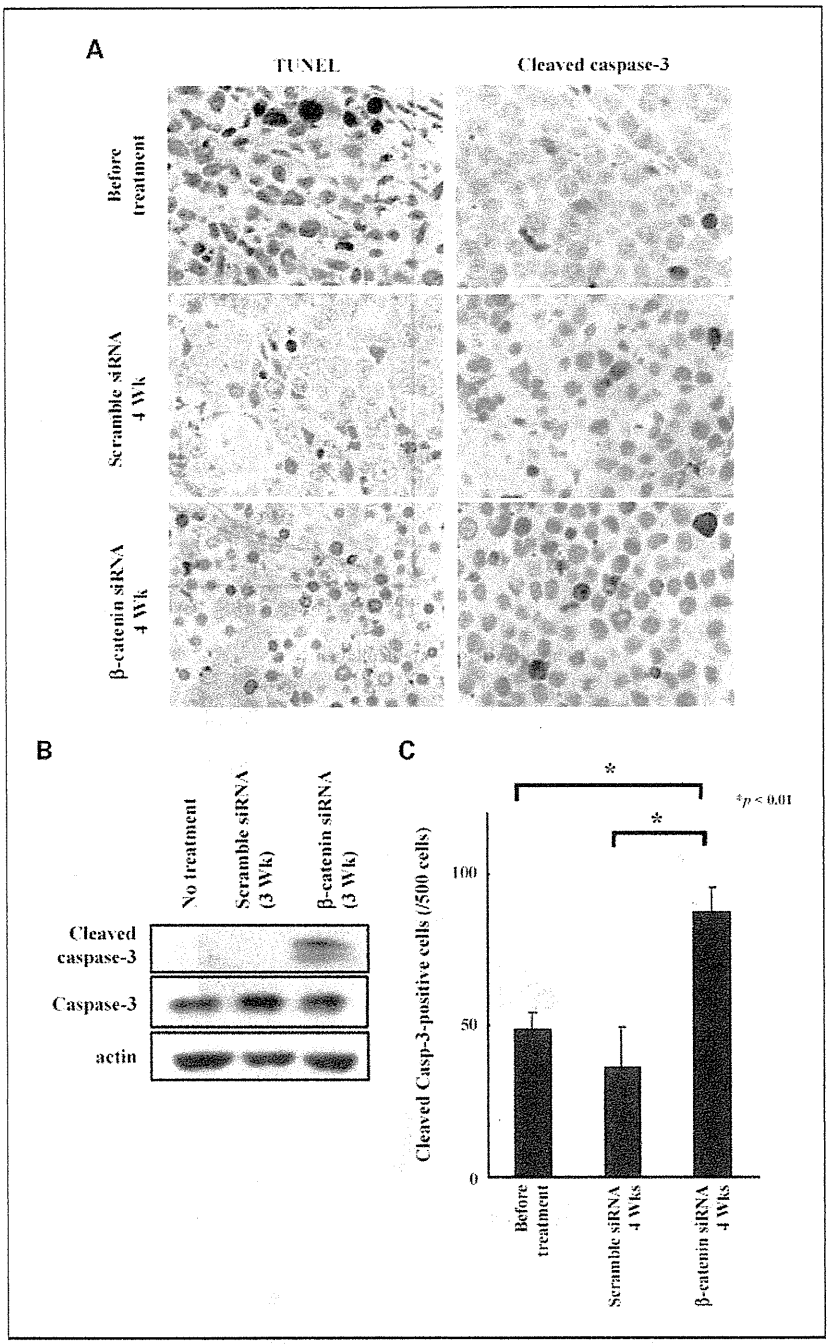

Fig. 4. Apoptotic cells and cleaved caspase-3 expression in myeloma tumors following treatment with β-catenin small interfering RNA. *A,* apoptotic cell (TUNEL-positive cell) numbers and cleaved caspase-3 expression increased following 4 wks of treatment with the β-catenin small interfering RNA/atelocollagen complex relative to before treatment and with the scramble small interfering RNA/telocollagen complex treatment. *B,* the expression of cleaved capsase-3 was increased in tumors after 3-wk treatment with β-catenin small interfering RNA/atelocollagen complex. *C,* cleaved caspase-3 positive cell numbers significantly increased in tumors of mice treated with β-catenin small interfering RNA/atelocollagen complex compared with those before treatment and those treated with scramble small interfering RNA/atelocollagen complex. Results are means ± SEs.

small interfering RNAs. In comparison with no treatment or treatment with scramble small interfering RNA, all three β-catenin small interfering RNAs caused a marked decrease in *β-catenin* mRNA levels (Fig. 2A). There were no significant differences in knockdown effects among three small interfering RNAs; therefore, β-catenin small interfering RNA 2 was used in further experiments. In A549 cells treated with β-catenin small interfering RNA 2, expression of *β-catenin* mRNA was reduced even at 72 hours after treatment, whereas no reduction was observed in non- or scramble small interfering RNA–treated cells (Fig. 2B). Similarly, β-catenin protein levels decreased after 72-hour treatment, whereas no reduction was observed in non- or scramble small interfering RNA–treated cells (Fig. 2C). These data showed that our β-catenin small interfering RNAs can diminish β-catenin expression successfully. Next, we investigated the antimyeloma effects of β-catenin small interfering RNA using a xenograft model.

In vivo *effects of β-catenin small interfering RNA on myeloma tumors.* We assessed β-catenin small interfering RNA–mediated growth inhibition *in vivo* using a mouse model (n = 3 per group). We administered β-catenin and scramble small interfering RNA/atelocollagen complexes twice a week for a total of eight injections and then compared expression of β-catenin and c-myc, as well as relative numbers of apoptotic

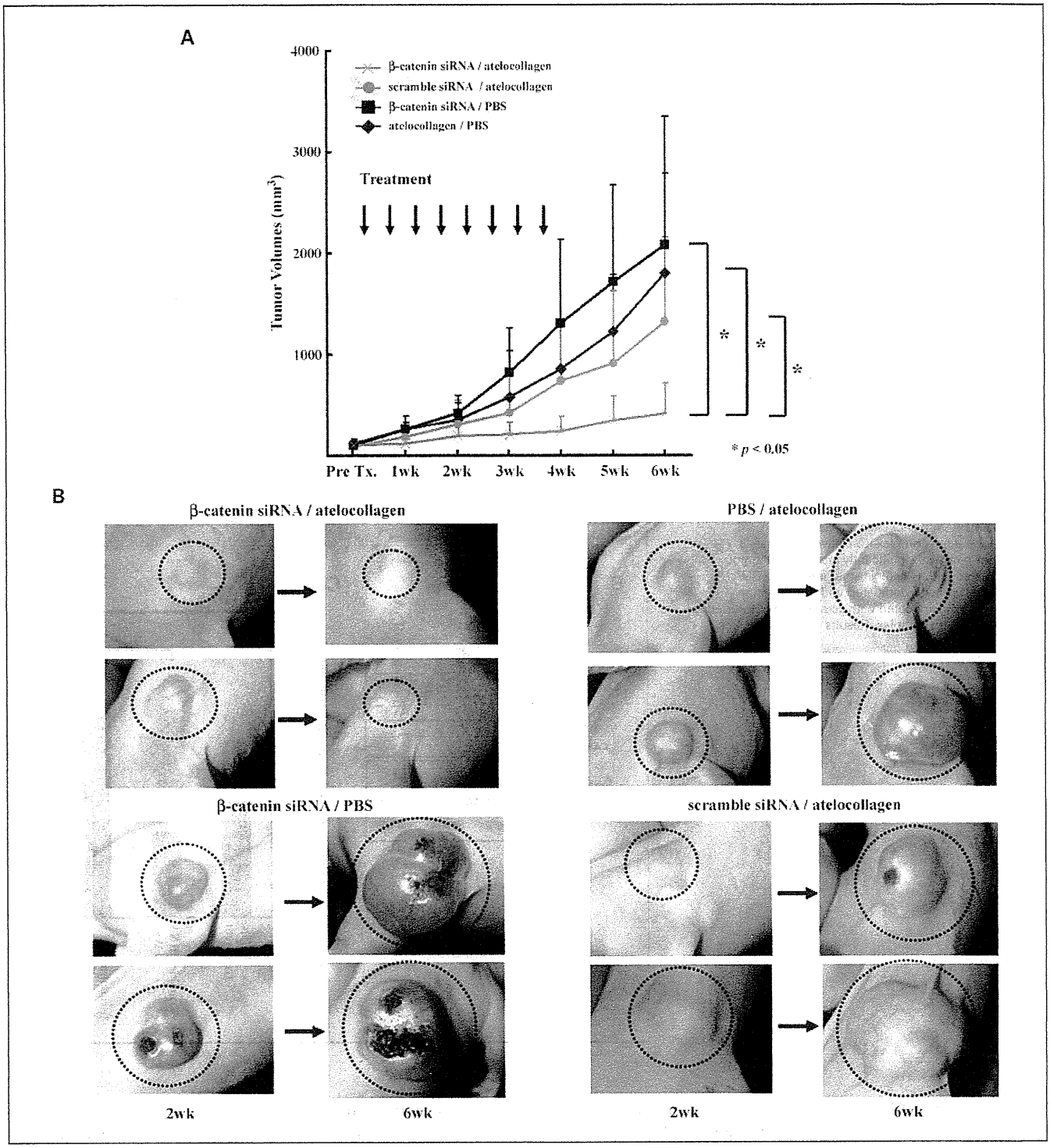

Fig. 5. Antimyeloma effects of β-catenin small interfering RNA in RPMI8226 xenografts. *A*, tumor growth curves. Palpable myeloma tumors (~100 mm^3 in volumes) were treated with s.c. (around the tumors) injections of β-catenin small interfering RNA (2.5 μmol/L)/1% atelocollagen complex (final atelocollagen concentration, 0.5%), scramble small interfering RNA (2.5 μmol/L)/1% atelocollagen complex, β-catenin small interfering RNA (2.5 μmol/L)/PBS, or PBS/1% atelocollagen twice a week for a total of eight injections (n = 5 per group). Treatment with β-catenin small interfering RNA/atelocollagen complex significantly reduced tumor volumes (P < 0.05). Results are means ± SEs. *B*, representative photos of tumor grafts after 2 and 6 wks of treatment. Dashed circles, myeloma tumors.

and cleaved caspase-3–positive cells. After RPMI8226 tumors had been treated for 1 or 2 weeks with the β-catenin small interfering RNA/atelocollagen complex, a significant decrease in *β-catenin* mRNA was observed (data not shown). After treatment for 4 weeks, β-catenin expression was decreased immunohistologically whereas expression was observed in tumors treated with the scramble small interfering RNA/atelocollagen complex (Fig. 3A, *left*). Because c-myc is a

target of β-catenin, we examined its expression in these 4-week-treated tissues (Fig. 3A, *right*). We found that, like β-catenin, c-myc expression was reduced significantly by treatment with the β-catenin small interfering RNA/atelocollagen complex (Fig. 3B and C). At this time point, we observed that the β-catenin small interfering RNA/atelocollagen complex–treated cells showed a significant increase in apoptotic cells using a TUNEL assay (Fig. 4A, *left*). To clarify the whether caspase was activated by the depletion of β-catenin, we investigated the expression of cleaved caspase-3 in multiple myeloma tumors by β-catenin small interfering RNA/atelocollagen complex treatment. Cleaved capase-3–positive cells were significantly increased in myeloma tumors treated with β-catenin small interfering RNA/atelocollagen complex treatment (Fig. 4A, *right*, and C). In Western analysis, cleaved caspase-3 was overexpressed in multiple myeloma tumors (Fig. 4B). Taken together, our results indicate that treatment with the β-catenin small interfering RNA/atelocollagen complex induced apoptosis of multiple myeloma cells by activating caspase-3.

Next, we evaluated the size of tumors during the 6 weeks following the treatment (n = 5 per group). At 6 weeks after treatment, the mean tumor volumes were as follows: β-catenin small interfering RNA/atelocollagen complex, 412.2 mm^3; scramble small interfering RNA/atelocollagen complex, 1,317.9 mm^3; β-catenin small interfering RNA/PBS, 2,075.9 mm^3; and PBS/1% atelocollagen, 1,802.3 mm^3. Treatment with the β-catenin small interfering RNA/atelocollagen complex significantly reduced tumor burdens and retarded tumor growth as measured by tumor volumes ($P < 0.05$; Fig. 5A and B). Therefore, these data show that the treatment with the β-catenin small interfering RNA/atelocollagen complex inhibits the proliferation of multiple myeloma tumors.

Discussion

In the present study, we used a mouse xenograft model to show that β-catenin small interfering RNA inhibits growth of multiple myeloma cells. To our knowledge, this is the first report showing that, for hematologic disorders, β-catenin small interfering RNA has growth inhibitory effects *in vivo*. Multiple myeloma cells are maintained and proliferate in the bone marrow through interactions between the bone marrow microenvironment and several cytokine growth factors for multiple myeloma cells, such as Wnt3a, Wnt5a, and Wnt10b (17). Activation of the canonical Wnt signaling pathway stabilizes β-catenin, and its nonphosphorylated form accumulates in the cytoplasm. β-catenin then translocates to the nucleus, where it interacts with T cell factor, driving transcription of target genes such as *c-myc* and *cyclin D1*. The mechanisms underlying aberrant β-catenin expression in multiple myeloma cells remain unclear. However, we have confirmed previous findings that suggested that multiple myeloma cells exhibit higher levels of β-catenin expression than normal hematopoietic cells (7, 9).

In various cancer therapies, RNA interference has been introduced experimentally and numerous methods for small interfering RNA transfection have been developed. At present, methods using viral vectors are the most efficient (18, 19). However, their utility is limited because of their potential to cause mutagenesis and develop cancers (20, 21). Several nonviral carriers have been developed for gene delivery, and atelocollagen is one of the most attractive of these novel carriers. It provides a clinically safe and readily available biomaterial (22).

Because atelocollagen has been developed as an *in vivo* drug delivery system (12, 14, 23, 24), we firstly confirmed the efficacy of three types of β-catenin small interfering RNAs *in vitro* using lipofection reagents as described previously (12, 24). Although small interfering RNAs could not be effectively transfected into myeloma cells *in vitro* (data not shown), our β-catenin small interfering RNAs decreased mRNA and protein levels of β-catenin in A549 and SW480 cells. We confirmed that our β-catenin small interfering RNAs could effectively induced RNA interference against β-catenin. Next, we evaluated the growth inhibition of myeloma cell tumors *in vivo* by β-catenin small interfering RNA/atelocollagen complex. After being administered around the tumors (enveloping the tumors), the β-catenin small interfering RNA/atelocollagen complex releases β-catenin small interfering RNA slowly, allowing it to diffuse into the tumors, where it silences β-catenin expression. We confirmed that treatment with the β-catenin small interfering RNA/atelocollagen complex diminished β-catenin and c-myc expression in immunohistological examinations. In addition, the expression of cleaved capsase-3 in multiple myeloma tumors was increased by the treatment of β-catenin small interfering RNA/atelocollagen complex, and significant increases in apoptotic and cleaved caspase-3–positive cells were observed in multiple myeloma tumors. Taken together, these results indicate that depletion of β-catenin induces apoptosis by activating capsase-3 and inhibit the growth of multiple myeloma cells.

In this study, we showed that the β-catenin small interfering RNA/atelocollagen complex inhibited proliferation of multiple myeloma tumors and that β-catenin might represent a molecular target for therapy against multiple myeloma. Small β-catenin inhibitor molecules have been developed and investigated, and preliminary findings have implicated β-catenin as a novel target for a cancer therapy (3, 9). Our data support these findings. However, because β-catenin is an important molecule for stem cell systems (25–27), systemic administration of β-catenin inhibitors might induce severe adverse effects. Moreover, Wnt/β-catenin signaling is essential for skeletogenesis, and it promotes osteoblast differentiation (28–30). Inhibition of Wnt/β-catenin signaling has been reported to result in the development of multiple myeloma bone disease(31, 32), whereas activation of the Wnt pathway suppresses the disease development (33). Supported by these results, a specific targeting strategy against these cells, such as antibody-combined small interfering RNA, is under investigation.

Disclosure of Potential Conflicts of Interest

No potential conflicts of interest were disclosed.

Acknowledgments

We thank Dr. Hiroyuki Yao for his excellent technical assistance and Dainippon Sumitomo Pharmaceutical (Osaka, Japan) and KOKEN Co. Ltd. (Tokyo, Japan) for providing atelocollagen.

References

1. He TC, Sparks AB, Rago C, et al. Identification of c-MYC as a target of the APC pathway. Science 1998;281:1509–12.
2. Tetsu O, McCormick F. Beta-catenin regulates expression of cyclin D1 in colon carcinoma cells. Nature 1999;398:422–6.
3. Lepourcelet M, Chen YN, France DS, et al. Small-molecule antagonists of the oncogenic Tcf/beta-catenin protein complex. Cancer Cell 2004;5:91–102.
4. Katoh M, Katoh M. WNT signaling pathway and stem cell signaling network. Clin Cancer Res 2007;13:4042–5.
5. Chung EJ, Hwang SG, Nguyen P, et al. Regulation of leukemic cell adhesion, proliferation, and survival by beta-catenin. Blood 2002;100:982–90.
6. Jamieson CH, Ailles LE, Dylla SJ, et al. Granulocyte-macrophage progenitors as candidate leukemic stem cells in blast-crisis CML. N Engl J Med 2004;351:657–67.
7. Derksen PW, Tjin E, Meijer HP, et al. Illegitimate WNT signaling promotes proliferation of multiple myeloma cells. Proc Natl Acad Sci U S A 2004;101:6122–7.
8. Serinsoz E, Neusch M, Busche G, Wasielewski R, Kreipe H, Bock O. Aberrant expression of beta-catenin discriminates acute myeloid leukaemia from acute lymphoblastic leukaemia. Br J Haematol 2004;126:313–9.
9. Sukhdeo K, Mani M, Zhang Y, et al. Targeting the beta-catenin/TCF transcriptional complex in the treatment of multiple myeloma. Proc Natl Acad Sci U S A 2007;104:7516–21.
10. Nogawa M, Yuasa T, Kimura S, et al. Intravesical administration of small interfering RNA targeting PLK-1 successfully prevents the growth of bladder cancer. J Clin Invest 2005;115:978–85.
11. Yano J, Hirabayashi K, Nakagawa S, et al. Antitumor activity of small interfering RNA/cationic liposome complex in mouse models of cancer. Clin Cancer Res 2004;10:7721–6.
12. Takei Y, Kadomatsu K, Goto T, Muramatsu T. Combinational antitumor effect of siRNA against midkine and paclitaxel on growth of human prostate cancer xenografts. Cancer 2006;107:864–73.
13. Zimmermann TS, Lee AC, Akinc A, et al. RNAi-mediated gene silencing in non-human primates. Nature 2006;441:111–4.
14. Minakuchi Y, Takeshita F, Kosaka N, et al. Atelocollagen-mediated synthetic small interfering RNA delivery for effective gene silencing *in vitro* and *in vivo*. Nucleic Acids Res 2004;32:e109.
15. Kuroda J, Kimura S, Segawa H, et al. The third-generation bisphosphonate zoledronate synergistically augments the anti-Ph+ leukemia activity of imatinib mesylate. Blood 2003;102:2229–35.
16. Kuroda J, Kimura S, Segawa H, et al. p53-independent anti-tumor effects of the nitrogen-containing bisphosphonate zoledronic acid. Cancer Sci 2004;95:186–92.
17. Dalton WS, Bergsagel PL, Kuehl WM, Anderson KC, Harousseau JL. Multiple myeloma. Hematology Am Soc Hematol Educ Program 2001:157–77.
18. Sumimoto H, Hirata K, Yamagata S, et al. Effective inhibition of cell growth and invasion of melanoma by combined suppression of BRAF (V599E) and Skp2 with lentiviral RNAi. Int J Cancer 2006;118:472–6.
19. Xu D, McCarty D, Fernandes A, Fisher M, Samulski RJ, Juliano RL. Delivery of MDR1 small interfering RNA by self-complementary recombinant adeno-associated virus vector. Mol Ther 2005;11:523–30.
20. Nienhuis AW, Dunbar CE, Sorrentino BP. Genotoxicity of retroviral integration in hematopoietic cells. Mol Ther 2006;13:1031–49.
21. Hacein-Bey-Abina S, Von Kalle C, Schmidt M, et al. LMO2-associated clonal T cell proliferation in two patients after gene therapy for SCID-X1. Science 2003;302:415–9.
22. Hanai K, Takeshita F, Honma K, et al. Atelocollagen-mediated systemic DDS for nucleic acid medicines. Ann N Y Acad Sci 2006;1082:9–17.
23. Takeshita F, Minakuchi Y, Nagahara S, et al. Efficient delivery of small interfering RNA to bone-metastatic tumors by using atelocollagen *in vivo*. Proc Natl Acad Sci U S A 2005;102:12177–82.
24. Kawata E, Ashihara E, Kimura S, et al. Administration of PLK-1 small interfering RNA with atelocollagen prevents the growth of liver metastases of lung cancer. Mol Cancer Ther 2008;7:2904–12.
25. Anton R, Kestler HA, Kuhl M. Beta-catenin signaling contributes to stemness and regulates early differentiation in murine embryonic stem cells. FEBS Lett 2007;581:5247–54.
26. Reya T, Duncan AW, Ailles L, et al. A role for Wnt signalling in self-renewal of haematopoietic stem cells. Nature 2003;423:409–14.
27. Fevr T, Robine S, Louvard D, Huelsken J. Wnt/beta-catenin is essential for intestinal homeostasis and maintenance of intestinal stem cells. Mol Cell Biol 2007;27:7551–9.
28. Bain G, Muller T, Wang X, Papkoff J. Activated beta-catenin induces osteoblast differentiation of C3H10T1/2 cells and participates in BMP2 mediated signal transduction. Biochem Biophys Res Commun 2003;301:84–91.
29. Westendorf JJ, Kahler RA, Schroeder TM. Wnt signaling in osteoblasts and bone diseases. Gene 2004;341:19–39.
30. Glass DA II, Bialek P, Ahn JD, et al. Canonical Wnt signaling in differentiated osteoblasts controls osteoclast differentiation. Dev Cell 2005;8:751–64.
31. Tian E, Zhan F, Walker R, et al. The role of the Wnt-signaling antagonist DKK1 in the development of osteolytic lesions in multiple myeloma. N Engl J Med 2003;349:2483–94.
32. Oshima T, Abe M, Asano J, et al. Myeloma cells suppress bone formation by secreting a soluble Wnt inhibitor, sFRP-2. Blood 2005;106:3160–5.
33. Edwards CM, Edwards JR, Lwin ST, et al. Increasing Wnt signaling in the bone marrow microenvironment inhibits the development of myeloma bone disease and reduces tumor burden in bone *in vivo*. Blood 2008;111:2833–42.

Lung Cancer 66 (2009) 75–79

Contents lists available at ScienceDirect

Lung Cancer

journal homepage: www.elsevier.com/locate/lungcan

Monitoring with a non-invasive bioluminescent *in vivo* imaging system of pleural metastasis of lung carcinoma

Seiji Matsumoto[a,c], Fumihiro Tanaka[a,c,*], Kiyoshi Sato[a,b], Shinya Kimura[b], Taira Maekawa[b], Seiki Hasegawa[c], Hiromi Wada[a]

[a] *Department of Thoracic Surgery, Faculty of Medicine, Kyoto University, Kyoto, Japan*
[b] *Department of Transfusion Medicine and Cell Therapy, Kyoto University Hospital, Kyoto, Japan*
[c] *Department of Thoracic Surgery, Hyogo Medical University, Mukogawa-cho1, Nishinomiya 663-8501, Japan*

ARTICLE INFO

Article history:
Received 16 July 2008
Received in revised form 8 December 2008
Accepted 10 December 2008

Keywords:
Pleural metastasis of lung carcinoma
Malignant pleural effusion
In vivo image system
Bioluminescence imaging
Intrapleural administration
Docetaxel

ABSTRACT

Objectives: The prognosis of patients with malignant pleural effusion (MPE) is poor. An MPE model is necessary for developing new therapeutic strategies. We established a MPE model and investigated the therapeutic effects of the administration of serial doses of docetaxel on intrathoracic disseminated foci using an *in vivo* image system (IVIS).
Methods: First, mice without pleural metastasis of lung carcinoma were given a single injection of docetaxel (Taxotere) in the thoracic cavity. The average weight of each group was evaluated. Next, docetaxel was injected into the thoracic cavity of the mice once a week for 8 weeks. Again, the average weight of each group was evaluated. Finally, A549 lung cancer cells transfected with luciferase gene (A549-Luc) were injected into the intrapleural cavity of the mouse. When pleural metastasis was established, we started repeated intrapleural administration of docetaxel (once a week for 8 weeks). The average weight of each group and the survival period was evaluated. All bioluminescent data were collected and analysed with a Xenogen IVIS® system.
Results: (1) Single administration study: The average weight of mice injected with 50 mg/kg docetaxel dropped 10%. (2) Repeat administration study: In the group of mice injected with 25 mg/kg or 50 mg/kg docetaxel, the average weight dropped by 10%. (3) A549-Luc cells were injected into the thoracic cavity of the mice. Autopsies revealed disseminated foci in thoracic cavity 7 days or more after inoculation. After confirmation of tumor formation, repeated injections of docetaxel were administered. After 21 days, photon counts from the thoracic cavity of untreated mice increased. Repeated intrapleural administration of docetaxel prolonged survival when compared to the control group.
Conclusions: (1) We established a MPE model. (2) IVIS® facilitates faster and more accurate counting of disseminated foci in the pleura (as compared to the previous standard of measuring body weight changes) in a cancerous pleuritis model. (3) Repeated intrapleural administration of docetaxel is effective.

1. Introduction

Malignant pleural effusion (MPE) is a common and life-threatening problem in patients with advanced malignancies such as primary lung cancer and breast cancer. The prognosis of patients with MPEs remains poor [1], and the mean survival period after confirming the diagnosis has been reported to be approximately 3 months. Patients often experience various manifestations caused by MPE, such as progressive dyspnea, cough, and chest pain, compromising the quality of the remaining short lifespan of these patients. In most cases, MPE is controlled by obliterating the pleural space (pleurodesis) which involves draining the fluid via a chest tube followed by intrapleural instillation of various sclerosing or chemotherapeutic agents [2]. However, pleurodesis sometimes fails to prevent re-occurrence of MPEs. This may result in higher rates of infection, as well as the need for repeated chest tube drainages and longer hospitalizations. Alternatively, prolonged placement of an indwelling pleural drainage catheter has been proposed for controlling MPEs [3,4]. Putnam et al. conducted a randomized study comparing placement of an indwelling pleural catheter with pleurodesis using doxycycline in the treatment of patients with MPE. They demonstrated that placement of an indwelling pleural catheter resulted in a shorter length of hospitalization for the patient.

Implantable access systems can be used for controlling malignant effusion. Such systems had been initially used for intraperitoneal administration of chemotherapeutic agents to control peritoneal effusion caused by malignant tumors such as ovarian

* Corresponding author. Tel.: +81 798 45 6885; fax: +81 798 45 6897.
E-mail address: ftanaka@hyo-med.ac.jp (F. Tanaka).

0169-5002/$ – see front matter © 2009 Published by Elsevier Ireland Ltd.
doi:10.1016/j.lungcan.2008.12.010

cancer [5–7]. Driesen et al. used an implantable access system for repeated intrapleural immunotherapy in patients with malignant mesothelioma [8].

Docetaxel, a taxane, is a newer chemotherapeutic agent that is widely used for the treatment of malignant tumors such as non-small cell lung cancer (NSCLC) and breast cancer. Docetaxel promotes microtubule polymerization and inhibits depolymerization, which results in a mitotic arrest in the G_2M phase of the cell cycle [9]. Docetaxel also induces apoptotic cell death by stimulating the phosphorylation of bcl-2 [10]. Many experimental studies showed that intravenous administration of docetaxel was effective in the treatment of mice bearing human cancer subcutaneous xenografts. In addition, one experimental study showed that intraperitoneal administration of docetaxel was safe and effective in the treatment of mice bearing ovarian carcinoma xenografts implanted intraperitoneally [11]. These results suggest that intrapleural docetaxel administration may be safe and effective for treating patients with MPE; however, safety and efficacy should be examined in animal models prior to clinical use.

In mice subcutaneous tumor models, tumor growth can be easily monitored by caliper measurements. However, in pleural metastasis models, it is difficult to measure tumor growth continuously and to evaluate response to a treatment. Surrogate markers such as weight loss may be employed to monitor toxicity, but the exact treatment efficacy is usually evaluated only after mice are sacrificed. In addition to computed tomography (CT), magnetic resonance imaging (MRI), and positron emission tomography (PET), an *in vivo* non-invasive bioluminescent imaging (BLI) system has recently been developed using the adenosine triphosphate (ATP)-dependent light-emitting reaction of the firefly (*Photinus pyralis*) luciferase and its substrate D-luciferin [D-(−)-2-(6′-hydroxy-2′-benzothiazolyl) thiazone-4-carboxylic acid] [12,13]. Using this system, temporal and spatial monitoring of pathophysiologic processes *in vivo* can be performed, therefore reducing the number of animals needed to achieve statistical power [12–19]. Thus, in this study, we first established pleural metastasis of lung carcinoma model, and then demonstrated the efficacy of intrapleural administration of docetaxel via continuous monitoring of pleural metastasis during the treatment using a non-invasive bioluminescent *in vivo* imaging system (IVIS).

2. Materials and methods

2.1. Cell line and animals

The human lung cancer cell line A549 (adenocarcinoma) was obtained from the American Type Culture Collection (ATCC, Rockville, MD). Cells were maintained at 37 °C in RPMI-1640 medium (GibcoBRL, Oaisley, Scotland) supplemented with 10% fetal calf serum (FCS) (Hyclone, Logan, UT).

Female BALB/c *nu/nu* mice were purchased from SLC Japan (Kyoto, Japan), and were maintained in a pathogen-free environment. All animal studies were performed in accordance with guidelines established by the Animal Welfare Committee of Kyoto University.

2.2. Evaluating the safety of intrapleural docetaxel administration

Docetaxel was a kind gift from Aventis Pharma Japan (Tokyo, Japan). A total of 42 five-week-old female BALB/c *nu/nu* mice were used in this study. There were 7 mice in each of the 6 treatment groups: 100 μl or 200 μl of saline, 5 mg/kg docetaxel in 100 μl or 200 μl of saline, or 50 mg/kg docetaxel in 100 μl or 200 μl of saline. To evaluate the safety of a single intrapleural administration of docetaxel, animals (bearing no tumor) were administered a single dose in the left pleural cavity and then maintained with no additional treatment. Body weights were measured twice a week to monitor toxicity.

2.3. Determining the optimal docetaxel dose in repeated intrapleural administration

Five-week-old female BALB/c *nu/nu* mice, bearing no tumor, were given weekly injections in the left thoracic cavity. Animals were treated at doses of 0 mg/kg, 1.0 mg/kg, 2.5 mg/kg, 5.0 mg/kg, 7.5 mg/kg, 10.0 mg/kg, 12.5 mg/kg, 25.0 mg/kg, or 50.0 mg/kg of docetaxel for 8 weeks (4 animals per treatment group). Each dose of docetaxel was dissolved in 100 μl of physiological saline. The optimal dose was defined as the maximum dose that did not cause treatment-related death or body weight loss of greater than 10% throughout the 8-week docetaxel treatment as well as the 8 weeks of follow-up.

2.4. Establishing A549 cell lines that express the firefly luciferase

A549 cells were co-transfected with the firefly luciferase gene (pGL3 Basic plasmid; Promega, Madison, WI) in combination with a vector for neomycin resistance, using Lipofectamine 2000 (Invitrogen, Carlsbad, CA). Cells were selected with G418 (Geneticin; Invitrogen). The surviving colonies were harvested and cultured independently. Cell clones were screened using a bioluminescence IVIS® (Xenogen). The A549 clone showing the highest luciferase activity (A549-Luc) was used in the present *in vivo* study. To evaluate how the number of cells effects the photon counts, A549-Luc cells were diluted to 1.0×10^5 cells per well, 5.0×10^4 cells per well, 2.5×10^4 cells per well, or 1.25×10^4 cells per well. Bioluminescence imaging with a charge-coupled device (CCD) camera (IVIS, Xenogen) was initiated 1–2 min after 150 μg/ml of D-luciferin (Xenogen) was added each well.

2.5. Treatment of pleural metastasis of lung carcinoma with intrapleural docetaxel injection

A549-Luc cells (5.0×10^6) were injected directly into the left pleural cavity of five-week-old female BALB/c *nu/nu* mice. IVIS was used to monitor the pleural metastasis of lung carcinoma. When establishment of pleural metastasis was ensured, mice were randomized into the control or docetaxel group (10 per group).

Mice in the docetaxel group received 8 weekly intrapleural injections of docetaxel at the previously determined optimal dose (10 mg/kg). Control mice were injected with the same volume (100 μl) of physiological saline on the same schedule as the docetaxel group. Pleural metastasis of lung carcinoma was monitored with IVIS.

2.6. Bioluminescence imaging with IVIS

Mice were anesthetized with isoflurane inhalation, and were subsequently intraperitoneally (i.p.) injected with 100 μl of 7.5 mg/ml D-luciferin (Xenogen). Bioluminescence imaging with a CCD camera (IVIS, Xenogen) was initiated 10 min after injection; imaging times ranged from 1 to 60 s, depending on the amount of luciferase activity. Bioluminescence from the region of interest (ROI) was defined manually, and the data were expressed as photon-flux (photons/s/cm^2/steradian). Background photon-flux was defined using an ROI from a mouse that was not given an i.p. injection of D-luciferin. All bioluminescent data were collected and analyzed using IVIS.

2.7. Statistics

The Stat View 5.0 statistical software package (SAS Institute Inc., Cary, NC) was used for all statistical analyses. The chi-squared test was used to compare photon counts. Continuous data between two groups were compared using: (1) Student's *t*-test, if the distribution of samples was normal, or (2) Mann–Whitney *U*-test, if the sample distribution was asymmetrical. Continuous data among three or more groups were compared using: (1) a one-way analysis of variance (ANOVA), if the distribution of samples was normal, or (2) the Kruskal–Wallis *H*-test, if the sample distribution was asymmetrical. The postoperative survival rate was analyzed by the Kaplan–Meier method, and the differences in survival rates were assessed by the log-rank test. Differences were considered significant when $p < 0.05$.

3. Results

3.1. Safety of single intrapleural injection of docetaxel

Female BALB/c *nu/nu* mice, five weeks in age and bearing no tumor, were administered a single injection of docetaxel (5 mg/kg or 50 mg/kg) in the left pleural cavity. Each dose was prepared in two dilutions using 100 μl or 200 μl of saline. Control mice were given 100 μl or 200 μl of saline alone. No deaths occurred in any of the 6 treatment groups. Although, no significant weight loss was observed after a single dose of 5 mg/kg docetaxel, a 10% decrease in weight was documented at 2 days following the injection of 50 mg/kg docetaxel (Fig. 1). The volume of saline used to prepare the docetaxel did not affect the weights of the mice; therefore, docetaxel was dissolved in 100 μl of saline in subsequent studies.

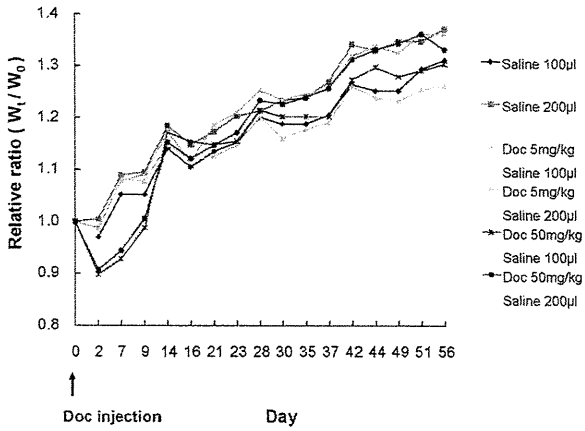

Fig. 1. Body weight changes after a single intrapleural injection of docetaxel Docetaxel was injected into the pleural cavity of non-tumor-bearing mice on Day 0. Docetaxel (Doc) was dissolved in 100 μl or 200 μl of physiological saline and administered at 0 mg/kg, 5 mg/kg, or 50 mg/kg. There were 7 mice in each group.

3.2. Determination of optimal dose for repeated intrapleural administration of docetaxel

To determine the optimal dose in repeated intrapleural administration of docetaxel for the treatment of pleural metastasis of lung carcinoma, mice were injected with docetaxel (0 mg/kg, 1.0 mg/kg, 2.5 mg/kg, 5.0 mg/kg, 7.5 mg/kg, 10.0 mg/kg, 12.5 mg/kg, 25.0 mg/kg, and 50.0 mg/kg) once per week for 8 weeks. Marked weight loss was observed in all mice administered 25 mg/kg or 50 mg/kg docetaxel. In addition, all mice in these treatment groups died before the completion of the 8 weekly injections (49 and 21 days respectively) (Fig. 2).

In contrast, no deaths or weight loss over 10% was documented in any group given a dose of 7.5 mg/kg docetaxel or less. At doses of 10–12.5 mg/kg of docetaxel, marginal weight loss was occasionally observed, but no deaths. Based on these results, we used 10 mg/kg of docetaxel in further repeated intrapleural treatment experiments.

3.3. Bioluminescent monitoring of pleural metastasis of lung carcinoma during treatment

A549 cells were transfected with the firefly luciferase gene, and plated at 1.0×10^5 cells per well, 5.0×10^4 cells per well, 2.5×10^4 cells per well, or 1.25×10^4 cells per well. Photon counts, as detected by IVIS, highly correlated to the number of cells in each well ($r^2 = 0.99$) (Fig. 3).

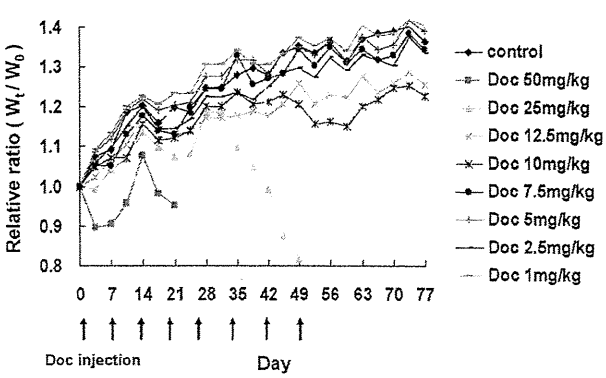

Fig. 2. Repeated intrapleural injections of docetaxel in non-tumor-bearing mice Docetaxel was administered weekly (Days 0, 7, 14, 21, 28, 35, 42, and 49) into the left pleural cavity of the mice. Docetaxel was dissolved in 100 μl of physiological saline and the mice were given a 0 mg/kg, 1 mg/kg, 2.5 mg/kg, 5 mg/kg, 7.5 mg/kg, 10 mg/kg, 12.5 mg/kg, 25 mg/kg, or 50 mg/kg dose. The day of first docetaxel injection is shown as Day 0. There were 4 mice in each group.

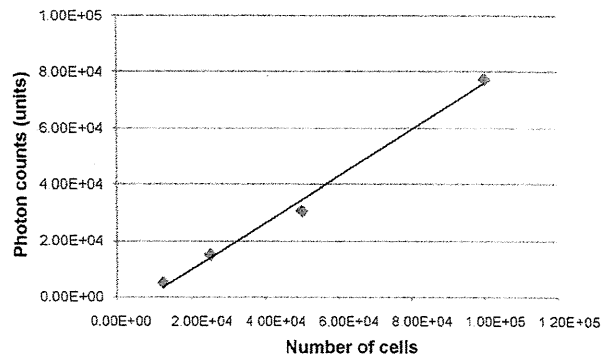

Fig. 3. Correlation of cell number and photon counts A549-Luc cells were diluted to 1.0 × 105 cells per well, 5.0 × 104 cells per well, 2.5 × 104 cells per well, and 1.25 × 104 cells per well and the photon counts were measured using a bioluminescent *in vivo* imaging system (IVIS) ($r2 = 0.99$).

A549-Luc cells (5×10^6) were injected into the left thoracic cavity of each mouse. Seven days after the cell implantation, establishment of pleural metastasis of lung carcinoma were confirmed using IVIS (Fig. 4(A)). Mice were then randomly divided into 2 treatment groups (control or 10 mg/kg docetaxel).

After treatment, pleural metastasis was monitored using IVIS (Fig. 4(A)); the photon intensity, a measurement of viable tumor volume, was also determined by the system (Fig. 4(B)). The average photon intensity did not increase following treatment with docetaxel; whereas, a significant increase in the photon intensity was observed in the control group (Fig. 4(A) and (B)).

Although 8 weekly intrapleural injections were initially planned, all mice in the control group died before "Day 49," the day of the 8th intrapleural injection. Autopsies revealed that all of the mice died due to enlargement of the pleural metastasis. All 10 mice in the docetaxel group survived until "Day 42" when the 7th intrapleural injection was scheduled. However, 2 of the 10 mice died just after the intrapleural injection was performed. Autopsies revealed that these mice had drug-induced interpleural adhesions and subsequently died of unintentional injuries to the lung during the intrapleural. Thus, we decided to not administer the 8th dose. The remaining 8 mice in the docetaxel group were sacrificed on "Day 53" (3 weeks after the final (7th) intrapleural injection of docetaxel). Autopsies revealed that 4 of these mice possessed drug-induced intrapleural adhesions; yet, virtually no disseminated tumor was observed in any mouse.

There was a significant survival advantage in the docetaxel group as compared with the control group ($p < 0.01$) (Fig. 5(A)). A slight increase in the average body weight was seen in the docetaxel group during repeated injections, but a significant (more than 10%) decrease was observed in the control group ($p < 0.01$) (Fig. 5(B)).

4. Discussion

In this study, we first established a pleural metastasis of lung carcinoma model. We then assessed the efficacy of repeated intrapleural injections of docetaxel by monitoring the tumors using the non-invasive IVIS.

In previous pleural metastasis models, tumor cells were injected into the pleural space of the mouse after skin and intercostal muscle incisions. This ensured that the tumor cells were implanted in the pleural space. In this study, however, intrapleural injections were performed without incisions. Our method was simple

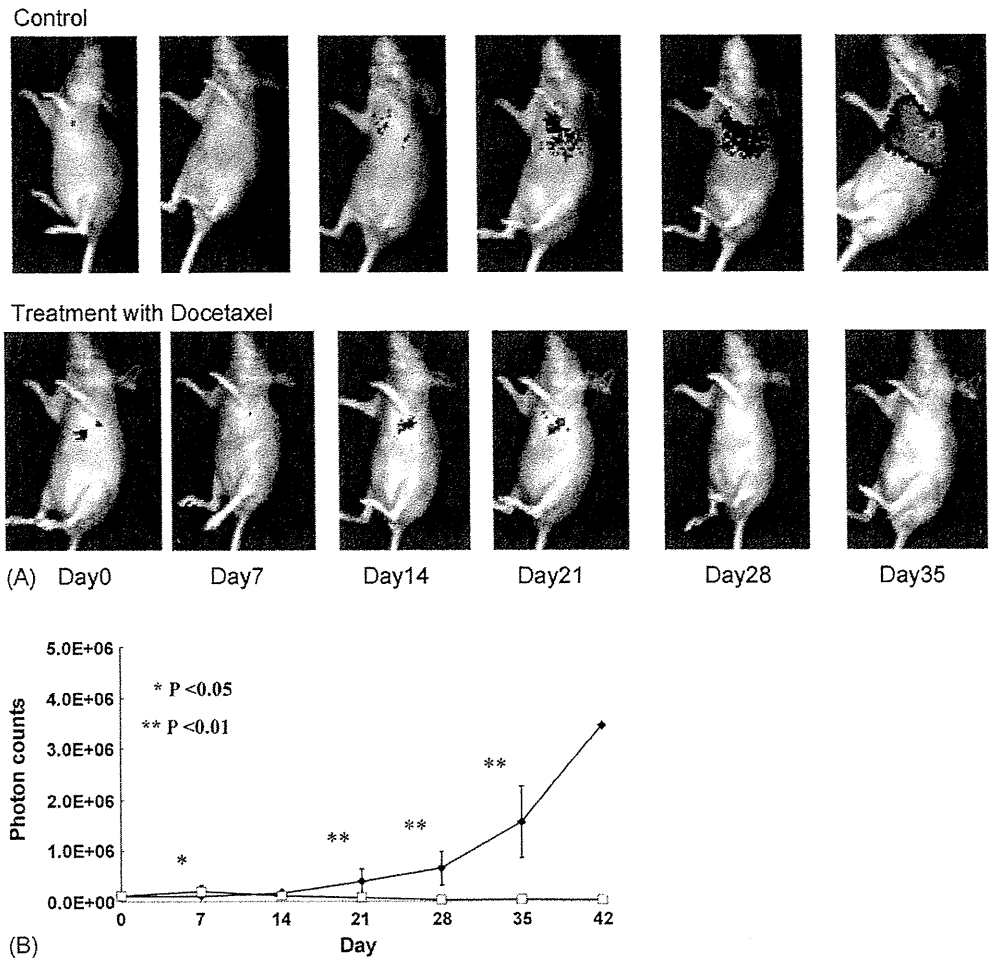

Fig. 4. Treatment of tumor-bearing mice with repeated intrapleural docetaxel injections A549-Luc cells (5 × 106) were injected into the left thoracic cavity of the mice. Seven days later, establishment of pleural metastasis of lung carcinoma was confirmed using a bioluminescent *in vivo* imaging system (IVIS). Mice were then randomized into a group with repeated intrapleural docetaxel treatment (10 mg/kg of docetaxel dissolved in 100 μl physiological saline) or a control group (the same volume of physiological saline). Pleural metastasis was monitored with the bioluminescent *in vivo* imaging system (A). The day of first docetaxel (or physiological saline) injection is defined as "Day 0." The bioluminescence intensity, a measurement of viable tumor volume, was also quantified by the system, and is indicated as photon-flux (photons/s/cm^2/steradian) (B).

as well as less invasive than the previous techniques. When evaluating the efficacy of treatment, it is essential that the tumor cells are consistently implanted in the intrapleural cavity prior to treatment. To address the issue, we used IVIS to ensure the establishment of pleural metastasis of lung carcinoma, as well as to monitor the efficacy of the treatments. In preliminary experiments, we attempted to establish pleural metastasis mouse models using the human lung cancer cell lines SBC-3, SBC-5, A549, and H1299 transfected with the firefly luciferase gene. Autopsies revealed that only the A549-Luc cell line consistently established disseminated tumors in all mice. Thus, we used the A549-Luc cell line to inoculate the thoracic cavity of the nude mice used in this study.

In a clinical trial, Shoji et al. performed repeated intrapleural administration of 5-FU and CDDP via a catheter in patients with MPE, and reported a favorable median survival of more than 1 year [20]. However, 5-FU was not active in lung cancer patients. More potent chemotherapeutic agents, such as docetaxel, have been developed in the 1990s. Therefore, we conducted an *in vivo* study to assess the safety and efficacy of intrapleural docetaxel treatment. First, we demonstrated that single or repeated intrapleural injections of docetaxel can be safely performed without inducing significant toxicities, especially acute hyperreaction. Next, we demonstrated a significantly prolonged survival in the docetaxel group as compared to the control animals. In addition, when autopsied, almost no pleural metastasis of lung carcinoma was observed in any mouse treated with docetaxel, whereas all mice in the control group died due to enlarged pleural metastasis. In our experiments, we clearly demonstrated that repeated intrapleural injections of docetaxel are safe and effective in our mouse model.

We repeatedly monitored the efficacy of docetaxel treatment using IVIS. A significant decrease in the average photon-flux count was observed during docetaxel treatment. Luminescence of luciferase requires both ATP and O_2; in addition, luminescence is not seen in necrotic sites. Therefore, photon-flux counts represent the volume of viable tumors. In our study, IVIS revealed a significant increase in the average photon-flux in the control mice on "Day 21," before any mice exhibited significant weight loss or died ($p < 0.01$). These findings indicate that IVIS is superior in speed and provides a more accurate representation of pleural metastasis. In conclusion, we established a pleural metastasis of lung carcinoma model using A549-Luc cells and demonstrated that the intrapleural administration of docetaxel may be a safe and effective treatment modality for MPE. Application of this treatment technique should be examined in clinical trials.

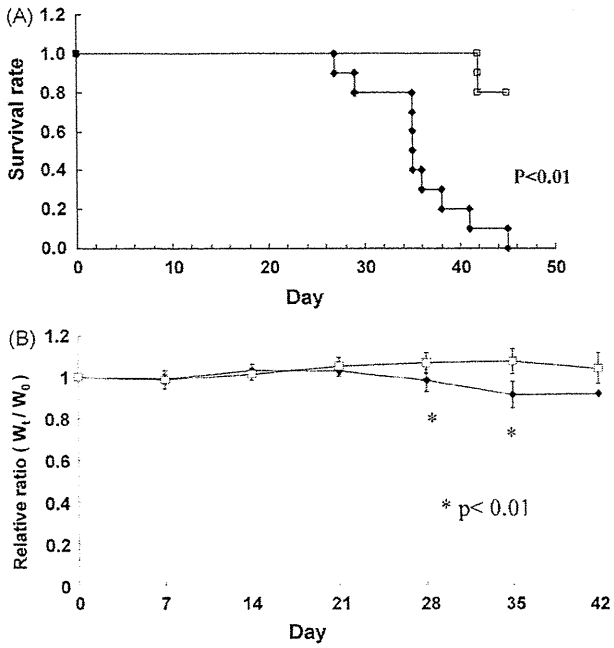

Fig. 5. Survival curves and relative body weight changes of the docetaxel treatment group and the control group are shown in (A) and (B), respectively. Repeated intrapleural docetaxel treatment significantly improved survival without inducing significant toxicities.

Conflict of Interest

None declared.

Acknowledgments

We gratefully acknowledge the contribution of Masaki Nogawa and the helpful comments of Philip C. Mack and Jamie McCall on several points in this paper.

References

[1] Sanchez-Armengol A, Rodriguez-Panadero F. Survival and talc pleurodesis in metastatic pleural carcinoma, revisited report of 125 cases. Chest 1993;104:1482–5.
[2] Light RW, Vargas FS. Pleural sclerosis for the treatment of pneumothorax and pleural effusion. Lung 1997;175:213–23.
[3] Putnam Jr JB, Light RW, Rodriguez RM, Ponn R, Olak J, Pollak JS, et al. A randomized comparison of indwelling pleural catheter and doxycycline pleurodesis in the management of malignant pleural effusions. Cancer 1999;86:1992–9.
[4] Putnam Jr JB, Walsh GL, Swisher SG, Roth JA, Suell DM, Vaporciyan AA, et al. Outpatient management of malignant pleural effusion by a chronic indwelling pleural catheter. Ann Thorac Surg 2000;69:369–75.
[5] Pfeifle CE, Howell SB, Markman M, Lucas WE. Totally implantable system for peritoneal access. J Clin Oncol 1984;2:1277–80.
[6] Malmstrom H, Carstensen J, Simonsen E. Experience with implanted subcutaneous ports for intraperitoneal chemotherapy in ovarian cancer. Gynecol Oncol 1994;54:27–34.
[7] Brandner P, Neis KJ. Use of an implantable catheter system for intraperitoneal chemotherapy in ovarian cancer. Artif Organs 1994;18:328–30.
[8] Driesen P, Boutin C, Viallat JR, Astoul PH, Vialette JP, Pasquier J. Implantable access system for prolonged intrapleural immunotherapy. Eur Respir J 1994;7:1889–92.
[9] Diaz JF, Andreu JM. Assembly of purified GDP-tubulin into microtubules induced by taxol and taxotere: reversibility, ligand stoichiometry, and competition. Biochemistry 1993;32:2747–55.
[10] Reed JC. Regulation of apoptosis by bcl-2 family proteins and its role in cancer and chemoresistance. Curr Opin Oncol 1995;7:541–6.
[11] Dykes DJ, Bissery MC, Harrison Jr SD, Waud WR. Response of human tumor xenografts in athymic nude mice to docetaxel (RP 56976 Taxotere). Invest New Drugs 1995;13:1–11.
[12] Contag CH, Bachmann MH. Advances in *in vivo* bioluminescence imaging of gene expression. Annu Rev Biomed Eng 2002;4:235–60.
[13] Edinger M, Cao YA, Hornig YS, Jenkins DE, Verneris MR, Bachmann MH, et al. Advancing animal models of neoplasia through *in vivo* bioluminescence imaging. Eur J Cancer 2002;38:2128–36.
[14] Sweeney TJ, Mailander V, Tucker AA, Olomu AB, Zhang W, Cao Y, et al. Visualizing the kinetics of tumor-cell clearance in living animals. Proc Natl Acad Sci USA 1999;96:12044–9.
[15] Vooijs M, Jonkers J, Lyons S, Berns A. Non-invasive imaging of spontaneous retinoblastoma pathway-dependent tumors in mice. Cancer Res 2002;62:1862–7.
[16] Adams JY, Johnson M, Sato M, Berger F, Gambhir SS, Carey M, et al. Visualization of advanced human prostate cancer lesions in living mice by a targeted gene transfer vector and optical imaging. Nat Med 2002;8:891–7.
[17] Laxman B, Hall DE, Bhojani MS, Hamstra DA, Chenevert TL, Ross BD, et al. Non-invasive real-time imaging of apoptosis. Proc Natl Acad Sci USA 2002;99:16551–5.
[18] Ray P, Pimenta H, Paulmurugan R, Berger F, Phelps ME, Iyer M, et al. Non-invasive quantitative imaging of protein-protein interactions in living subjects. Proc Natl Acad Sci USA 2002;99:3105–10.
[19] Ciana P, Raviscioni M, Mussi P, Vegeto E, Que I, Parker MG, et al. *In vivo* imaging of transcriptionally active estrogen receptors. Nat Med 2003;9:82–6.
[20] Shoji T, Tanaka F, Yanagihara K, Inui K, Wada H. Phase II study of repeated intrapleural chemotherapy using implantable access system for management of malignant pleural effusion. Chest 2002;121:821–4.

Mod Rheumatol (2009) 19:431–436
DOI 10.1007/s10165-009-0171-3

CASE REPORT

Severe erosive arthropathy requiring surgical treatments in systemic lupus erythematosus

Toshiyuki Kitaori · Hiromu Ito · Hiroyuki Yoshitomi · Tomoki Aoyama · Takao Fujii · Tsuneyo Mimori · Takashi Nakamura

Received: 28 November 2008 / Accepted: 17 March 2009 / Published online: 14 April 2009

Abstract We report a case of 43-year-old woman with an overlap syndrome of systemic lupus erythematosus (SLE) and dermatomyositis who developed erosive arthritis with extracapsular cysts involving multiple joints. An extensive synovectomy for the left wrist joint and a total joint replacement for the right hip joint were required to achieve complete symptom relief. She was not diagnosed with rheumatoid arthritis (RA). This was a rare case of SLE manifesting non-RA erosive arthritis that required surgical interventions.

Keywords Systemic lupus erythematosus (SLE) · Erosive arthritis · Rheumatoid arthritis · Surgical treatment

Introduction

Arthritis is a prominent symptom in systemic lupus erythematosus (SLE) patients and forms 1 of the original 11 American College of Rheumatology (ACR) criteria for the classification of the disease [1, 2]. Reportedly, 40–60% of SLE patients suffer from joint involvement. Arthropathy associated with SLE is commonly nonerosive, which is differentiated from that of rheumatoid arthritis [1, 2]. Histopathologically, joint synovitis is only occasionally observed and the arthropathy lacks pannus formation or bone erosion, because the SLE arthropathy mainly comes from an inflammation with fibrosis of the joint capsule [3–5]. However, several groups have described erosive arthritis in SLE. A study reported that 1.6% of SLE patients have erosive arthropathy [6]. Fernandez et al. [7] reported eight patients who had erosive arthropathy with clinical findings similar to rheumatoid arthritis (RA), which they called "rhupus" arthropathy. However, the pathology and clinical course of erosive arthropathy in SLE patients is not well described. Herein we report a case of erosive arthropathy accompanied by extracapsular cysts for which surgical treatments were required.

T. Kitaori · H. Ito (✉) · H. Yoshitomi · T. Nakamura
Department of Orthopaedic Surgery, Kyoto University Graduate School of Medicine, 54 Shogoin-Kawaharacho, Sakyo-ku, Kyoto 606-8507, Japan
e-mail: hiromu@kuhp.kyoto-u.ac.jp

T. Fujii · T. Mimori
Department of Rheumatology and Clinical Immunology, Kyoto University Graduate School of Medicine, 54 Shogoin-Kawaharacho, Sakyo-ku, Kyoto 606-8507, Japan

T. Aoyama
Institute for Frontier Medical Sciences, Kyoto University, 53 Shogoin-Kawaharacho, Sakyo-ku, Kyoto 606-8507, Japan

Case report

A 38-year-old woman was admitted to our department in September 2003 with an annoying symptom of growing tumorous lump with pain on her left wrist. The patient had been previously diagnosed with an overlapping syndrome of dermatomyositis (DM) and SLE with symptoms and abnormalities as follows: Gottron sign, heliotrope eruption, increased creatine kinase (CK) and aldolase (ALD), myogenic change in electromyography, myositis at histopathology, polyarthritis, malar rash, positive antinuclear antibody (ANA), and hypocomplementemia in 2002. Since then she had been treated with 10–20 mg/day of prednisone. When admitted, physical examination demonstrated a $5 \times 10 \times 3$ cm^3 elastic soft tumor on the dorsal aspect of the left wrist (Fig. 1a). There was tenderness at the distal ulna. There was no pulsation or thrill on the tumor. The

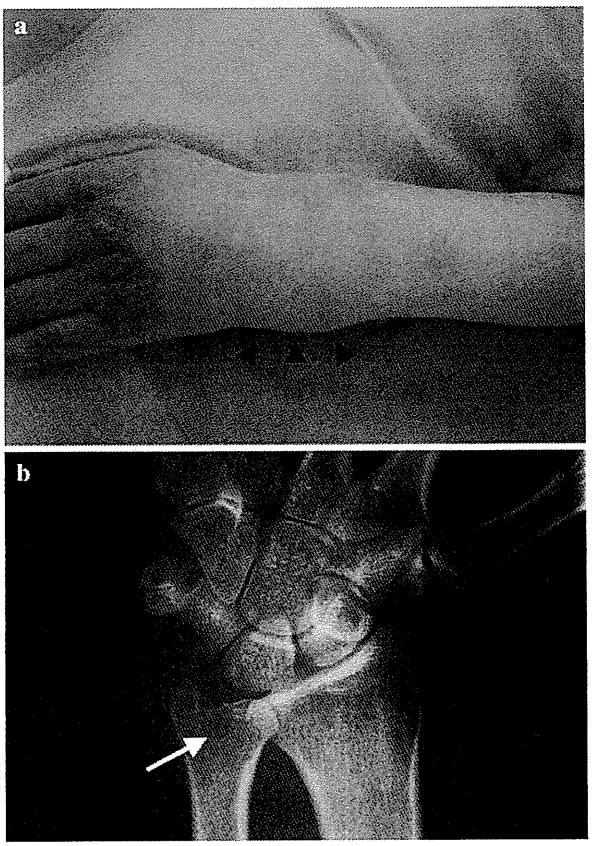

Fig. 1 Clinical manifestation and X-ray of the left wrist joint. **a** Left hand with an elastic soft tumor on its dorsal aspect (*arrowheads*), **b** X-ray. An *arrow* indicates the erosive lesion of the distal ulna

range of motion of the wrist joint was normal when compared with the other side, while there was pain on motion. Finger functions were not disturbed.

Laboratory examinations revealed that erythrocyte sedimentation rate (ESR) was 34 mm/h, white blood cell (WBC) count was 7,200/μl (neutrophilic cells 90.0%, basophilic cells 1.0%, monocytes 4.0%, lymphocytes 3.0%, atypical lymphocytes 1.0%, myelocytes 1.0%), platelet count was 15.2 × 10^4/μl, and hemoglobin was 11.2 mg/dl. Liver enzymes were within normal ranges except for elevated lactate dehydrogenase (LDH) of 344 (129–241) IU/L. Renal and coagulation functions were normal. Immunological data showed positive antinuclear antibody (1:160, speckled pattern with positive cytoplasmic staining). Anti-double strand DNA (dsDNA) antibody rose to 8.6 (normal <6.0) IU/ml at its peak. Rheumatoid factor (RF) and anticyclic citrullinated peptide (anti-CCP) antibodies were both negative. Complements were all decreased: C3 37.7 (70.5–125.6), C4 2.4 (10.6–33) mg/dl, and CH_{50} 11.1 (28–51) U/ml. Urinary protein was negative. X-ray revealed slight bone erosion of distal ulna (Fig. 1b). Ultrasound imaging showed that the lump was cystic. Wrist T1- and T2-weighted magnetic resonance imaging (MRI) revealed extracapsular cyst and mass formation around the distal ulna (Fig. 2a).

Because the cyst became larger, the patient underwent surgical excision of the extracapsular cyst in July 2004. The cyst contained yellow and cloudy fluid and had a thin connection into the wrist joint. After the excision of the cyst, curettage of the wrist joint was performed through the pinhole resulted from the excision. Histopathological study revealed that the mass consisted of synovium. After the surgery, however, continuous exudate from the wound lasted for a month before complete wound closure. Shortly afterwards the cyst reappeared. Reoperation with more extensive excision was performed in September 2004, but the cyst reappeared again. The second MRI demonstrated that the synovium around the distal ulna reached to the triangular fibrocartilage complex (TFCC) and eroded into the distal ulna (Fig. 2b). In November 2004, on the third operation, the TFCC was partially excised and the synovium was completely eradicated from the wrist joint through both dorsal and palmar arthrotomies, after which there has been no recurrence, with no dysfunction of the wrist joint except for the surgical scar. Histopathological analysis demonstrated nonspecific and chronic joint synovitis by the following findings: eosinophilic amyloid-like deposition surrounded by epithelioid macrophages, negative amyloid staining, and necrotic tissue with the infiltration of inflammatory cells including neutrophils (Fig. 3a). There were no findings of infection or malignancy.

Meanwhile, she had also noticed a lump on the right inguinal lesion since 2003. X-ray (Fig. 4a left) and MRI (Fig. 4b) studies in January 2005 revealed extracapsular cysts around the right hip joint without any findings of joint destruction. She did not have any symptoms except for a huge mass around the medial aspect of the right thigh, and 65 ml yellow and cloudy fluid was aspirated from the cyst in March 2005, which resembled that observed in the left wrist joint. For the aggravating synovitis, additional treatment with 6 mg/week methotrexate (MTX) was started, but this medication was stopped 2 months later because of gastrointestinal discomfort. MTX was switched to 1 mg/day tacrolimus, which has been continued since then. Despite the additional medication, she developed right hip pain 2 years later. In September 2007, X-ray (Fig. 4a right) and another MRI (Fig. 4c) revealed joint space narrowing of the right hip joint, fluid collection, and expanding synovium-like tissue which expanded from the joint cavity towards the extracapsular cysts. No findings indicated aseptic necrosis of femoral head (AVN). Due to the increasing pain and limited morbidity, total hip replacement (THR) was performed in 2008. Histological analysis of the hip joint revealed damaged joint cartilage and bared subchondral bone of femoral head, but without any findings

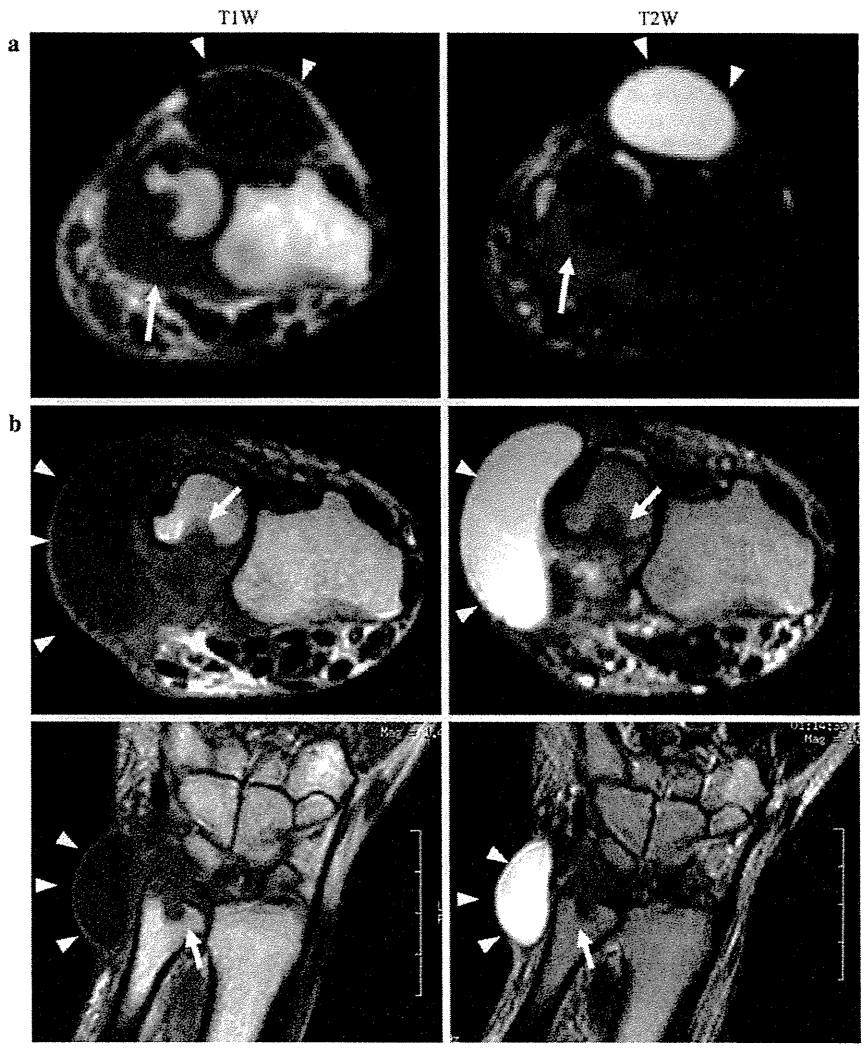

Fig. 2 T1-weighted (*left*) and T2-weighted (*right*) MR images before the first (**a**) and third (**b**) operations. **a** Axial MR images showing extracapsular cyst (*arrowheads*) and mass formation around the distal ulna (*arrows*). **b** Axial (*top*) and coronal (*bottom*) MR images demonstrating extracapsular cyst (*arrowheads*) and eroding synovium into the distal ulna (*arrows*)

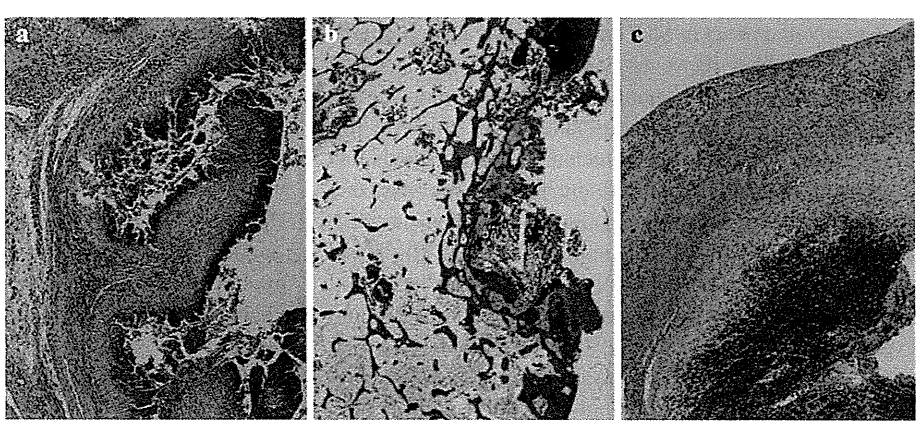

Fig. 3 Histological examinations. **a** Hematoxylin and eosin (H&E) stain of the synovium of the left wrist joint (*bar* 200 μm). **b**, **c** H&E stain of the articular surface of femoral head (**b**) and the synovium of the right hip joint (**c**) (*bar* 1 mm)

of osteonecrosis (Fig. 3b). The synovitis lacked lymph follicle formation or rheumatoid nodule (Fig. 3c). These findings were similar to those of the wrist joint, only demonstrating nonspecific synovial arthritis (Fig. 3a). She became completely free from symptoms after the operation.